Physics – Uspekhi **54** (4) 351 – 370 (2011)

REVIEWS OF TOPICAL PROBLEMS PACS numbers: 07.77.Gx, **36.40. – c**, 36.40.Ei, 42.62.Fi, 81.07.Nb, 82.50.Hp

Kinetic methods for measuring the temperature of clusters and nanoparticles in molecular beams

G N Makarov

DOI: 10.3367/UFNe.0181.201104b.0365

Contents

Abstract. The temperature (internal energy) of clusters and nanoparticles is an important physical parameter which affects many of their properties and the character of processes they are involved in. At the same time, determining the temperature of free clusters and nanoparticles in molecular beams is a rather complicated problem because the temperature of small particles depends on their size. In this paper, recently developed kinetic methods for measuring the temperature of clusters and nanoparticles in molecular beams are reviewed. The definition of temperature in the present context is given, and how the temperature affects the properties of and the processes involving the particles is discussed. The temperature behavior of clusters and nanoparticles near a phase transition point is analyzed. Early methods for measuring the temperature of large clusters are briefly described. It is shown that, compared to other methods, new kinetic methods are more universal and applicable for determining the temperature of clusters and nanoparticles of practically any size and composition. The future development and applications of these methods are outlined.

1. Introduction

Investigations of clusters and nanoparticles are currently one of the most rapidly developing areas of fundamental physics [1–39]. (To recall, clusters with the number of particles $N \geqslant 10^2$ and nanoparticles are the same aggregates or ensembles of particles [39–41]). Due to the discrete structure of energy levels and high surface-to-volume ratio, clusters and nanoparticles have peculiar properties that distinguish them from both their constituent components and the bulk substance. Quantum and structural, as well as dimensional and surface, effects are of importance in such small systems. Considerable interest in the investigation of clusters and nanoparticles arises from their unique properties, dimensional effects, and a variety of nanotechnological applications [42, 43] to manufacture miniature high-speed electronic devices and systems with high-capacity memory, to deposit thin films, and to develop new materials and treat their surfaces [1, 18, 20, 29, 31]. Further, an increasingly greater interest in metallic and composite clusters and nanoparticles is attributable to the possibility of using them as new high-temperature superconductors [36, 44–47]. Such applications of clusters and nanoparticles require deep knowledge of their physical, chemical, and thermodynamic properties.

Temperature (internal energy) is one of the most important physical characteristics of clusters and nanoparticles, responsible for many of their properties and the character of processes in which they happen to be involved (see, for instance review [35] and references cited therein). Hence, there is great importance in developing methods for the diagnostics of clusters and nanoparticles, including those for measuring their temperature. However, the creation of a 'thermometer' to measure the temperature of free clusters and nanoparticles in molecular beams encounters rather serious difficulties. Recently, a few kinetic methods for measuring the temperature of clusters and nanoparticles in molecular beams have been proposed. The present work is designed to consider these techniques.

The review cutline is as follows. Section 2 deals with the temperature of clusters and nanoparticles. The kinetic and

G N Makarov Institute of Spectroscopy, Russian Academy of Sciences, ul. Fizicheskaya 5, 142190 Troitsk, Moscow region, Russian Federation
Tel. (7-496) 751 02 32. Fax (7-496) 751 08 86
E-mail: gmakarov@isan.troitsk.ru

Received 21 April 2010, revised 17 June 2010
Uspekhi Fizicheskikh Nauk **181** (4) 365 – 387 (2011)
DOI: 10.3367/UFNr.0181.201104b.0365
Translated by Yu V Morozov; edited by A Radzig

thermodynamic definition of cluster temperature is proposed. The temperature behavior of clusters and nanoparticles near a phase transition point is analyzed. The influence of temperature on cluster properties and its role in physicochemical processes with the participation of clusters and their beams is discussed. Section 3 contains a synopsis of early methods for measuring the temperature of clusters and nanoparticles, such as the electron diffraction method and optical and thermodynamic methods. Estimates of cluster temperature are reported as obtained in experiments on gas (or vapor) outflow from a nozzle in the absence of gas-carriers. The basis of the method for measuring the temperature of clusters and nanoparticles is considered in the framework of the evaporative ensemble concept. Advantages and disadvantages of these methods are analyzed. Results of studies on temperature distribution in small clusters stabilized by evaporation are presented.

The central Section 4 focuses on the recently developed kinetic methods for measuring the temperature of free clusters and nanoparticles in molecular beams. Basic principles of these methods are described along with the experimental data on the temperature of alkali metal clusters. Results of experiments on measuring the temperature of van der Waals $(CF_3I)_N$ clusters in a beam are presented. A universal probe method for measuring the temperature of large clusters (nanoparticles) in a beam is described in considerable detail, which is based on using miniature probe thermometers (molecules or atoms) placed on the cluster surface. The results of measurements of the temperature of $(CO_2)_N$ nanoparticles in a cluster beam by this method are presented. Detailed analysis of the possibilities of kinetic methods for measuring the temperature of clusters and nanoparticles, and prospects for their further development and application are presented. The closing Section 5 reports the main results of the studies reviewed in this paper and their possible implications.

2. The temperature of clusters and nanoparticles and its influence on particle properties

The temperature of clusters and nanoparticles and the methods for its measurement and stabilization are considered at great length in Ref. [35] (see also the recent review [39]). In addition, these works contain analysis of the influence of the temperature on particle properties and the character of processes in which particles participate. Therefore, only brief mention is made here of the main facts concerning the temperature of clusters and nanoparticles that may be helpful in understanding the issues considered in this work. Notice that it is devoted to new kinetic methods for measuring the temperature of free clusters and nanoparticles in molecular beams that were developed recently and were not yet discussed in the aforementioned publications [35, 39].

Cluster (nanoparticle) temperature is determined by the energy of random motion of constituent atoms or molecules with respect to the cluster's center of masses. When the rotational and translational degrees of freedom of a cluster are 'frozen', its internal temperature $T_{\rm cl}$ is given by the relation

$$\frac{3N}{2}\,k_{\rm B}T_{\rm cl}=\left\langle\sum_{i=1}^{N}\frac{m_i(v_{\rm c.m.}-v_i)^2}{2}\right\rangle, \qquad (2.1)$$

where m_i and v_i are the mass and velocity of constituent atoms (molecules), $v_{\rm c.m.}$ is the velocity of the cluster's center of masses, N is the number of particles in the cluster, and $k_{\rm B}$ is the Boltzmann constant.

Relation (2.1) actually represents the kinetic definition of the cluster temperature. Alternatively, it can be defined as a thermodynamic quantity:

$$T_{\rm cl}=\frac{{\rm d}E}{{\rm d}S}\,, \qquad (2.2)$$

where E and S are the total internal energy and entropy of the cluster, respectively. The temperatures defined by expressions (2.1) and (2.2) are different quantities and discrepancy between them may have serious consequences (see Refs [30, 38, 48, 49] and references cited therein). The thermodynamic consideration of clusters takes account not only of the energy of thermal motion of their atoms, but also of the potential energy of atom–atom interactions inside the cluster [30, 35, 38, 39], including configuration excitation energy. By configuration excitation is meant transitions of a cluster from the ground state to local minima of a multidimensional space of the potential energy surface. It is configuration excitations that change the cluster structure and aggregate state [19, 30, 35, 38, 39, 48, 49].

The thermodynamic definition of cluster temperature is more accurate and complete. The thermodynamic consideration of clusters taking account of their total internal energy and entropy permits us to describe many processes associated with structural transitions and provides an in-depth understanding of phase transition physics in clusters [30, 35, 38, 39, 49]. By way of example, this approach allowed the negative heat capacity of a cluster near the melting point to be predicted [50–55]. Experimentally, the negative heat capacity was observed in papers [56–61].

It should be noted that the introduction of a thermodynamic parameter (temperature) for a cluster as a system of a finite number of particles (as opposed to a bulk material) is problematic; it requires substantiation and elaboration. Both in experiment and computer simulations, a cluster may be regarded as a canonical or microcanonical ensemble of atoms, meaning that the cluster resides either in isothermal or adiabatic conditions. Isothermal conditions are implied for the cluster temperature given by relations (2.1) and (2.2), whereas adiabatic conditions correspond to beam expansion into a vacuum and many other conditions of cluster studies. As shown below, it is in the adiabatic conditions that configuration excitation changes the cluster temperature. The cluster negative heat capacity observed near the melting point also occurs under adiabatic conditions. It is rather specific in character owing to cluster phase coexistence near the melting point. We will briefly discuss these questions below on a qualitative level.

The characteristic feature of clusters and nanoparticles (small-sized systems) is the fact that the coexistence of liquid and solid states in them takes place in some region of temperatures in the vicinity of the melting point [19, 30, 38, 39, 49, 62–76]. The results of theoretical studies and computer simulations dating back to the 1970s [77–81] show that clusters composed from atoms and molecules exist in two (or more) stable states corresponding to solid and liquid forms. Under proper conditions, these states may correspond to other forms, e.g., glassy-like [30, 82] or slush-like [48, 63, 71–73]. The coexistence of phases means that a cluster is alternatively a solid or a liquid. Therefore, the behavior of atoms in the cluster is characterized by at least two effective (mean) temperatures corresponding to the solid and liquid

states [30, 38, 39, 49, 75], the typical time for the establishment of thermal equilibrium in a cluster between atomic vibrations being much smaller than the transition time between the two aggregate states. Given that a time longer than the time the cluster resides in either of the phase states is considered, the cluster can be characterized by a single temperature determined by statistical thermodynamic averaging over a large time interval. These three temperatures are not significantly different [30, 49, 75] [see also relation (2.8)].

These peculiarities of cluster temperature can be understood from the relationship between thermal and configuration excitations of a cluster under adiabatic (isoenergetic) conditions, when it is just a microcanonical ensemble of atoms. In this case, equilibrium between the cluster atoms depends on the hierarchy of times needed to come into the equilibrium. In the approximation of two aggregate states [83], the typical time τ_{eq} of thermal equilibration between bound atoms inside the cluster is on the order of [30, 75]

$$\tau_{eq} \sim \frac{1}{\omega_D} , \tag{2.3}$$

where ω_D is the Debye frequency inversely proportional to the vibration period of cluster atoms ($\sim 10^{-14}$ s at $T \approx 300$ K). The typical time τ_{ag} of cluster transition between the aggregate states is large compared to τ_{eq}:

$$\tau_{eq} \ll \tau_{ag} , \tag{2.4}$$

because such transition requires a high energy barrier to be overcome [30, 38, 49].

Let us consider a cluster as a microcanonical ensemble of bound atoms and disregard its interaction with the environment; in other words, let us assume that

$$\tau_{ag} \ll \tau_{th} , \tag{2.5}$$

where τ_{th} is the typical time of energy exchange between the cluster and its environment. For times shorter than τ_{th}, the cluster may be regarded as an isolated particle. Let us introduce the typical time τ of cluster observation, such that

$$\tau_{ag} \ll \tau \ll \tau_{th} . \tag{2.6}$$

This hierarchy of times [relations (2.4)–(2.6)] leads to the specific picture of cluster evolution and determination of its temperature. Indeed, the thermal equilibrium between vibrations of cluster atoms is reached for time τ_{eq}; then, their thermal motion can be characterized by the temperature [84]. Criterion (2.4) implies that this temperature is different for two aggregate states, which makes it possible to introduce separate temperatures, T_{sol} and T_{liq}, for atoms of solid and liquid states of the cluster [30, 38, 39, 49, 65, 70, 76]. Specifically, the cluster energy in the Dulong–Petit limit is given by the expression [30, 49]

$$E = (3N - 6)\, k_B T_{sol} = \Delta E_{mel} + (3N - 6)\, k_B T_{liq} , \tag{2.7}$$

where ΔE_{mel} is the cluster melting energy. Hence it follows that

$$\Delta T = T_{sol} - T_{liq} = \frac{\Delta E_{mel}}{(3N - 6)\, k_B} . \tag{2.8}$$

For large times on the order of τ, the total cluster temperature T_{cl} can also be introduced. It can be expressed in terms of the average energy of individual cluster atoms [relation (2.1)] if averaging is taken over a sufficiently large time (on the order of τ), during which the cluster can repeatedly change its aggregate state.

Unless a cluster interacts with the environment, the thermodynamic equilibrium is established inside it. Then, the total cluster temperature can be introduced based on the thermodynamic relation (2.2), in addition to the temperatures of solid and liquid aggregate states. This relation can be used to determine both temperatures of each aggregate state and the mean cluster temperature averaged over large time [30, 49].

Thus, for a cluster residing in microcanonical (adiabatic) conditions, the above differentiation of cluster evolution times makes it possible to separately determine temperatures of the solid and liquid aggregate states of the cluster [84]. These states under canonical (isothermal) conditions can also be given by different mean kinetic and potential energies [30, 49, 75]. However, a single cluster temperature can be used if the cluster observation time exceeds the typical time for which the dynamic equilibrium between the aggregate states is reached [30, 49, 75].

The effective temperature of a cluster, either solid or liquid, in an ensemble with a constant energy can be estimated in either of the two ways: either through the mean kinetic energy of the particles or through the derivative of the internal energy with respect to the entropy at constant volume. Whereas these two methods are equivalent for determining the temperature in the case of a canonical ensemble of macroscopic systems, they may be not at all equivalent for microcanonical ensembles, in particular, of small systems, such as clusters and nanoparticles. The effective temperature of the solid state defined in terms of kinetic energy must surpass that of the liquid state at the same energy [see relation (2.8)]. This means that a rise in the cluster energy in the region of coexistence of solid and liquid states (near the phase transition point) may result in a drop in its effective temperature. Under the above conditions in the phase transition region, when equilibrium is reached at each new cluster energy, any small rise in this energy near the melting point is used partially to excite the thermal (vibrational) motion of the particles and partly to induce configuration excitation. Consequently, the heat capacity of an isolated cluster changes in the vicinity of the melting point. Moreover, the process becomes possible where a part of the cluster internal kinetic energy is expended on configuration excitation together with a new portion of the energy previously delivered from outside. In this case, the cluster temperature decreases with increasing energy; in other words, the cluster possesses negative thermal capacity near the melting point [30, 38, 39, 49, 75].

As mentioned above, transition from the solid aggregate state to the liquid one is associated with configuration excitation of the cluster. This implies an occurrence of configuration temperature responsible for this excitation [30, 49, 75]. At zero temperature, only that configuration component of the cluster energy, which corresponds to cluster excitation with respect to the global minimum of the potential energy surface, is preserved. At high temperatures, the kinetic energy of atomic motion may be significantly higher than the configuration excitation energy. These issues, as well as phase transitions in clusters, cluster evolution near phase transition points, and cluster temperatures, are discussed at great length in the studies by R S Berry and his group [30, 48, 49, 63–73, 75, 76, 82, 83], D J Wales [52, 53, 67, 74, 85–87], and B M Smirnov [9, 30, 38, 48, 49, 75, 82, 83] (see reviews and monographs [9, 19, 30, 38, 70, 86, 87] and references cited therein).

The temperature of clusters depends on their type (composition) and modes of formation and stabilization; it is subject to wide variations [35, 39]. For example, the temperature of ^{3}He and ^{4}He clusters stabilized by evaporation is 0.15 and 0.38 K, respectively [88, 89]. That of noble gas clusters in molecular beams or aggregates ranges, as a rule, from a few to tens of kelvins. Molecular clusters (including those with hydrogen bonds) have a temperature between several dozen and one or several hundred kelvins. The temperature of metal and carbon clusters (including fullerenes) prepared by laser irradiation or under gas discharge conditions may be as high as approximately 3500–4000 K, and that of refractory metal clusters reaches 4500–5000 K. Under equilibrium conditions, the upper limiting temperature of a cluster depends on the melting point of the cluster substance [35, 39].

Cluster temperature is an important physical parameter playing an important role in many physicochemical processes involving clusters and cluster beams [35]. It determines the polarizability and magnetic moments, ionization potentials, structure, and optical properties of clusters. Temperature influences many other properties of clusters and processes with their participation [90, 91], such as charge transfer processes during collisions between cluster ions and metal atoms, which are dominated in chemical reactions [92, 93].

Fragmentation channels in collisions of clusters and cluster ions with atoms and solid surfaces also depend on cluster temperature [13, 31, 35]; the same is true of energy relaxation mechanisms, namely, fragmentation, emission of charged particles (electrons and ions), and radiation of light [31, 35, 94, 95]. Cluster temperature has a marked effect on the reaction rate between clusters and other reactants [96, 97] and on the rate and pathways of chemical reactions at the surface or inside large ($N \geqslant 10^3$) van der Waals clusters [25, 28, 98–101].

The deformation and mobility of clusters at a surface also depend on their temperature [102–104], for example, in the formation of nanostructures on the surface and deposition of cluster films [103, 104]. Large clusters ($N \geqslant 10^3$) with high internal temperatures easily undergo deformation when deposited on a hot surface, giving rise to two-dimensional structures. It was demonstrated by the molecular dynamics method [103] that deposition of $YBa_2Cu_3O_{7-x}$ clusters with $N = 10^3$ and temperature $T_{cl} \geqslant 2400$ K onto the surface of pyrolytic graphite resulted in the formation of a film no more than two atomic layers thick. Nanometer-sized hot clusters were shown to be readily deformed on a solid surface due to the high internal energy, and they transform from three-dimensional into two-dimensional structures. Such transformation occurs even on a surface at room temperature [104]. High cluster energy enables atoms to easily overcome the existing local potential barriers and reorientate at the surface so as to form a high-quality film. Such technology opens up the possibility of forming thin films of superconducting materials.

3. A brief survey of early methods for measuring the temperature of clusters and nanoparticles. Temperature distribution in small clusters

3.1 Early methods for measuring the temperature of clusters and nanoparticles

There are a number of methods for measuring the temperature of clusters and nanoparticles [35]: the electron diffraction method [105–109]; detection of equilibrium emission from excited or heated clusters [110–113]; measurement of the temperature of the substrate at which the clusters are absorbed [114, 115]; determination of the temperature of clusters generated in nozzle sources without a gas-carrier based on the thermodynamic parameters of the cluster substance [116–123], and measurement of the temperature of excited clusters and those undergoing fragmentation from the kinetic energy of taking-off fragments [122–125]. Worthy of special mention is a unique precision method for measuring the temperature of large clusters (nanodroplets) of superfluid helium-4 from the infrared (IR) absorption spectra of incorporated molecules [24, 26–28, 126].

The electron diffraction method [105–109] takes advantage of the intersection between electron and cluster beams, with the former giving rise to diffraction rings [105]. The ring diameter permits lattice parameters to be determined, which in turn may be used to determine the lattice temperature by comparison with the characteristics of the bulky material. Size effects in the clusters are also taken into account. However, this method is applicable only to clusters that undergo crystallization into the same phase as the bulky substance. For example, an inert gas cluster has to consist of 10^3 or more atoms if the method in question is to be employed because smaller clusters have a quasicrystalline icosahedral structure, rather than a close-packed crystalline one (see review [35] and references cited therein).

Measurement of cluster temperature based on the detection of equilibrium radiation [110–113] is used for hot or excited clusters. It should be emphasized that the clusters formed by the majority of known techniques (laser irradiation, sputtering, pulse discharges, hot vapor expansion) are hot unless they cool in collisions with the gas-carrier. An additional excitation of clusters by intense laser radiation [110–112, 127–130], electron impact [113, 131–134], energetic ions [135, 136], collisions with a solid surface [13, 31], or chemical reactions [137] carries them to highly excited states. The excitation energy rapidly transforms into heat due to a high density of states, and the cluster heats up rather strongly. Like any 'blackbody', a hot cluster emits light. The radiation spectra allow the internal temperature of emitting clusters, as well as their heating and cooling rates, to be determined with a rather high accuracy [35].

The temperature of clusters deposited or condensed on a surface depends on the latter's temperature ($T_{cl} = T_s$) [114, 115, 138–143]. Clusters may also form and cluster layers grow on a cold surface [114, 115, 142–146]. Surface (and cluster) temperature may vary in a wide range, depending on the cluster type (composition) to be formed and stabilized. Cluster formation on a cold surface is possible using both atomic and molecular beams and fluxes of a laser-sputtered substance and a rarefied gas present in the chamber at a low pressure [35].

Determination of cluster temperature from the kinetic energy of taking-off fragments is based [122, 123] (see also Sections 4.2 and 4.3) on the fact that the mean kinetic energy ε^* with which an atom or molecule leaves the cluster surface is a measure of the temperature of the transient cluster state. If the fragmentation process is described by the hard-sphere model, this relationship is given by the expression [122, 123]

$$\varepsilon^* = k_B T_{cl}^* , \tag{3.1}$$

where T_{cl}^* is the cluster temperature in the transient state. However, the temperature measured by this method for small

clusters is lower than the temperature of the fragmentating parent cluster because part of its energy is spent to evaporate the monomer [122, 123]. Notice also that the measurement of the kinetic energy of dissociation fragments forms the basis for the determination of cluster temperature by the methods considered in the present review (see Section 4).

An original method for measuring the temperature of laser-excited clusters (and of their melting heat and temperature) has been developed by Haberland and co-workers [56–59, 147, 148] (see also review [39] and references cited therein). The authors focused on the thermal properties of clusters and used laser excitation to obtain the caloric curves (temperature dependences of cluster energy) for mass-selected sodium ion clusters in a beam. The experimental caloric curves allowed estimating the melting temperature and heat of clusters of a known size and their temperature upon laser excitation. The clusters themselves served in measuring their temperature as highly sensitive calorimeters. Two mass spectrometers were used in the experiments: one to select clusters of the desired size, and the other to analyze their fragmentation either by laser excitation or heat treatment. The basic idea behind the experiments is as follows [56, 58, 147]. A cluster having temperature T_1 is heated to T_2, when it absorbs a laser photon with energy $\delta E = h\nu$. When thus excited, the cluster undergoes fragmentation and has a certain mass spectrum. The resulting cluster temperature T_2 can be determined from the cluster source temperature due to its rise till the heat-treated clusters begin to display the same fragmentation pattern (i.e., the same mass spectrum) as the laser-heated ones. In other words, the above authors determined the temperature of laser-excited clusters by comparing the fragmentation patterns of clusters having identical internal energy under conditions of laser excitation and nozzle heating.

A unique method for measuring cluster temperature was applied to nanodroplets (clusters) of superfluid helium. It determines the temperature of nanodroplets from IR absorption spectra of the molecules incorporated in them [24, 26–28, 126]. This method is the most straightforward and accurate. Molecules almost freely rotate inside the superfluid helium droplets, which accounts for the appearance of a rotational structure in the IR absorption spectra that can be used to estimate the population of the molecular rotational levels and, therefore, the molecule's temperature inside the cluster. The resulting temperature is refined from a comparison of observed and predicted spectra [26–28, 126].

Considerable progress in the investigation and measurement of cluster temperature was achieved by analysis of cluster cooling by evaporation [116, 117] and the introduction of the notion of an 'evaporative ensemble' [118–124]. Gspann [117] proposed characterizing clusters produced in nozzle sources on the assumption that they undergo intense evaporation and that the evaporation rate constant is the inverse of the time interval between successive events of the evaporation process. Moreover, he hypothesized that the expression for the evaporation rate constant k_{ev} follows a form analogous to the Arrhenius formula:

$$k_{ev} = A \exp\left(-\frac{\Delta E_{ev}}{k_B T_{cl}}\right), \tag{3.2}$$

where ΔE_{ev} is the evaporation energy (heat) per particle. Expression (3.2) establishes the relationship between cluster energy ΔE_{ev} and temperature on the assumption that the pre-exponential factor A is a universal constant. Bearing in mind this formal relation, it is possible to determine the temperature of the clusters being evaporated. The values thus obtained are consistent with experimental ones [35, 39, 116, 123]. At the same time, clusters prepared by other methods (e.g., sputtering, laser ablation, and gas discharges) needed to be described as well. The properties of these small aggregates (clusters and nanoparticles) were also found to be dependent on the evaporation process. The procedure proposed by Gspann was further developed and improved in the work of Klots [118–123]. Simulation of the evolution of small systems required working out of more general approaches [119]. One of them was the evaporative ensemble model described in paper [118].

Klots considered cluster temperature in terms of the theory of monomolecular reactions [149, 150]. However, cluster dissociation (evaporation) processes are usually described in terms of the system's energy instead of temperature. Evaporation rate constants were accurately calculated in papers [119, 122]. These calculations are based on the evaluation of temperature-dependent (canonical) evaporation rate constants used to obtain microcanonical (particle energy-dependent) rate constants. The main result of the above studies, directly related to the problem under consideration, indicates that the temperature of the aggregate being evaporated (cluster or nanoparticle) can be rather accurately estimated [123] (see also review [35]) from the following relation

$$k_B T_{cl} \approx \frac{\Delta E_{ev}}{G}, \tag{3.3}$$

where G is Gspann's parameter [35, 39, 122, 123] equaling approximately 25–30, which depends not at all on the cluster material [35, 122, 123].

An important contribution to the investigation of evaporative cluster cooling and the development of the relevant theory was made by K Hansen and coworkers [151–157] (see also Section 3.2). Purposeful implication of the evaporation process provided a basis for the elaboration of the most efficacious and productive methods of cluster physics. The evaporative ensemble concept proved to be of special value for the investigation of size-dependent variations of cluster stability and the collection of information about their inner structure [7, 158]. Specifically, this approach was utilized to study stability variations of clusters depending on their electron shell structure [159, 160]. The evaporation method was also employed to estimate the activation (dissociation) energy of sodium clusters [156, 157] and to explore cluster plasmon absorption [161].

Expression (3.3) establishes the relationship between cluster temperature and evaporation heat. At the same time, the cluster temperature is by no means a constant quantity, as it may seem from Eqn (3.3). It depends on the cluster size because it also determines the energy of evaporation of atoms (or molecules) from the cluster surface (see, for instance, reviews [35, 39] and references cited therein).

To conclude this section, cluster temperature is related to the intermolecular interaction potential between atoms (molecules) inside the cluster [35]. The stronger the interatomic attraction in a cluster, the higher its temperature, and conversely the weaker the interatomic attraction, the lower the final temperature of the cluster. This relationship is consistent with condensation and evaporation processes in cluster beams [35, 39, 162].

3.2 Temperature (internal energy) distribution in small clusters

The development of the evaporative ensemble theory produced a number of very interesting results [116–124, 151, 155]. The most important one is that an ensemble of clusters of a given size is characterized by a specific temperature (internal energy) distribution. Another interesting result reduces to the statement that the cluster temperature at a given instant can be rather accurately estimated if the time that elapsed from the onset of cluster cooling due to evaporation is known (even when its starting temperature remains unknown) [116–124, 151, 155].

The key to understanding the problem of cluster internal energy (temperature) became the observation of low heat capacity of clusters due to their small size. This makes cluster evaporation a stepwise process, unlike the continuous evaporation of macroscopic substance. A cluster cools appreciably even during a single evaporation event. Moreover, the measurement time under usual experimental conditions is much greater than the pre-exponential time in the expressions for thermally activated processes [35, 39, 116, 117]. For this reason, the cluster temperature is significantly lower than the activation energy of evaporation [see, for instance, relation (3.3)]. With these facts in mind, it may be safely suggested that two successive events of evaporation from one and the same cluster may have rate constants differing by a few orders of magnitude.

This inference is schematically illustrated in Fig. 1a showing evaporation of a 50-atom sodium cluster [151]. At each step, the cluster loses one atom and cools by an activation energy of about 0.9 eV for the process [156, 157].

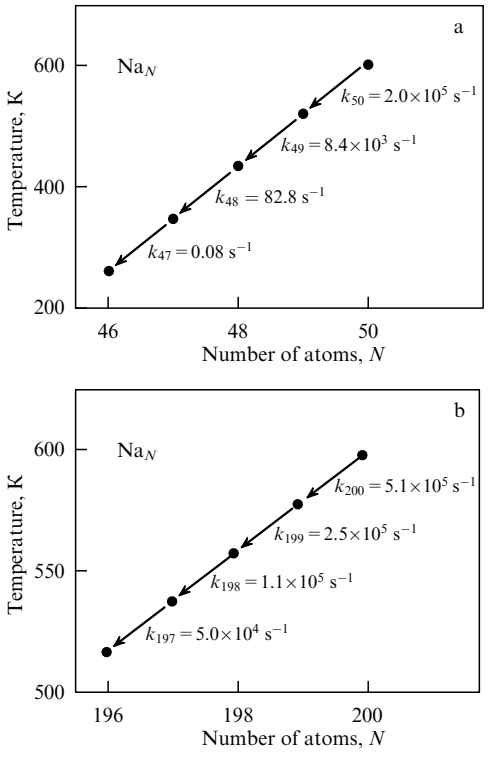

Figure 1. (a) The sequence of several events of atomic evaporation from an Na_{50} cluster. Evaporation of only a few atoms results in a dramatic change in cluster temperature. It drops from 600 to 400 K for less than 1 ms [151]. (b) The sequence of several events of atomic evaporation from an Na_{200} cluster. The evaporation rates are commensurate, in contrast to Fig. 1a.

Because the evaporation rate exponentially depends on the cluster temperature [see formula (3.2)], even a minor change in temperature strongly influences the rate of further evaporation. The heat capacity of a small-sized cluster being low, its temperature drops significantly with each evaporation event; also, the probability of further evaporation decreases from one step to the next by orders of magnitude. A different scenario is realized for larger clusters (Fig. 1b). By way of example, a sodium cluster of 200 atoms cools in each evaporation event less significantly (roughly by 20 kelvins) and the evaporation rates along the sequence differ only by a factor of 2 or so, rather than 100-fold, as in Fig. 1a. Evidently, larger clusters undergo a progressively smaller drop in temperature in each successive event of evaporation as their size increases, while the evaporation rates in further occurrences are practically identical.

Thus, the last stage in a chain of small-cluster decays comprising a few evaporation steps always needs more time to be realized and dominates on the time scale (see Fig. 1a). Consequently, the time spent for the last evaporation step is the effective time of the entire cluster-cooling process. This well-established relationship between cooling time and evaporation rate implies a maximum evaporation rate at each moment in an ensemble of clusters of a given size. Knowing the maximum evaporation rate, it is possible to deduce (using, for example, formula (3.2)) the well-defined upper limit, $T_{\max}$, for cluster temperature distribution. Higher-temperature clusters are too hot to remain in a given state during cooling. They release atoms and are therefore absent in the ensemble of clusters of a given size.

On the other hand, there is a minimum temperature $T_{\min}$ for clusters of this size, depending on the decay of clusters of the preceding size in the chain. Evidently, such clusters also have an upper temperature limit. Clusters with a temperature above this maximum value will evaporate during cooling. In other words, the lowest temperature of clusters of size N corresponds to the highest temperature of clusters of size $N+1$ minus the drop in temperature due to evaporation of a single particle [151]. Because the maximum temperature of two adjacent clusters in the decay chain is essentially the same (given the same activation energy), the difference between the maximum and minimum temperatures is given by the temperature drop ΔT in a single evaporation event. Evidently, this quantity depends on the cluster evaporation energy and heat capacity and (disregarding the kinetic energy of the evaporated particle) is given by the expression

$$k_{\mathrm{B}}\Delta T = \frac{\Delta E_{\mathrm{ev}}}{(3N-6)} \approx \frac{\Delta E_{\mathrm{ev}}}{3N}\,, \tag{3.4}$$

where ΔE_{ev} is the evaporation energy or activation threshold, N is the number of atoms in the cluster, and $(3N-6)$ is the number of the cluster's vibrational degrees of freedom.

On these assumptions, all peculiarities of the final energy (temperature) distribution of clusters that were initially hot and showed wide energy distribution can be deduced by considering only the last evaporation step. For small-sized clusters, a roughly rectangular temperature distribution bounded by the values of $T_{\max}$ and $T_{\min}$ is formed (Fig. 2). The width of this temperature distribution is $k_{\mathrm{B}}\Delta T \approx \Delta E_{\mathrm{ev}}/3N$. As shown in Fig. 2a, the distribution of large clusters ($N \geqslant 100$) over energies has a Gaussian shape. It becomes narrower with increasing cluster size, and the difference between $T_{\max}$ and $T_{\min}$ tends to zero. This means

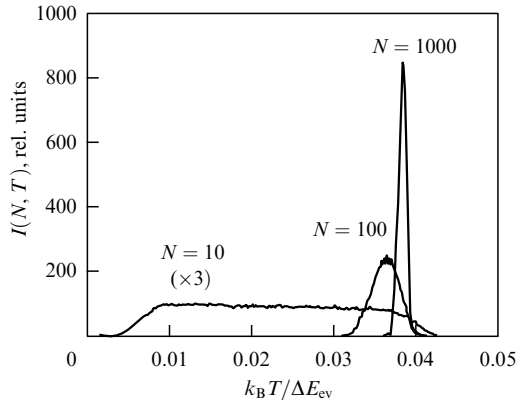

Figure 2. Temperature distributions for clusters of size $N = 10$, 100, and 1000 calculated by the Monte Carlo method. The distribution is almost flat for $N = 10$ (magnified by a factor of 3) but has a Gaussian form for $N = 100$, and 1000 [151].

that the temperatures of the nearest similar-sized clusters, as well as the rates of successive evaporation steps, are virtually identical for large clusters. These are important conclusions from the evaporative ensemble theory [121, 151], which must be taken into account in the experimental determination of small-sized cluster and nanoparticle temperatures.

4. Kinetic methods for measuring the temperature of clusters and nanoparticles

The kinetic methods for measuring the temperature of free clusters and nanoparticles in molecular beams are based on the measurement of the kinetic energy of fragments produced in evaporation (dissociation) of hot or laser-excited clusters [122–123]. The cluster temperature is also possible to determine by measuring the internal energy of evaporated fragments (molecules, dimers) [125, 151]. As mentioned in Section 3.1, the mean kinetic energy ε^* with which an atom or molecule leaves the cluster surface may be a measure of temperature of the cluster transient state. Therefore, the temperature of a decomposing cluster can be found from the measured kinetic or internal energy (quantum state) of dissociation products [122, 123] and by measuring the recoil (deflection) and escape of large daughter fragments from the beam. Both approaches were employed in the methods considered below.

4.1 Measuring the temperature of Na_N clusters from the recoil pattern of fragmentation products

In this section, we consider the method for determining the temperature of neutral Na_{20} clusters, which is based on a measurement of the recoil (escape from the beam) energy of daughter fragments produced in the course of cluster evaporation [124]. The essence of the method is as follows. The clusters forming in an ultrasonic expansion source are irradiated by a laser at a certain distance from the input aperture of the beam detector. By varying this distance and simultaneously measuring variations in ion peak intensities of the mother cluster and daughter fragments, it is possible to identify fragmentation channels and obtain information about the temperature of the initial cluster and its fragments.

The authors of work [124] chose the Na_{20} cluster as a model system for the following reasons. First, Na_{20} is a well-studied cluster having a filled shell. Second, it represents the dominant magic number in the sodium mass spectrum; its abnormally high content compared with that of the nearest similar-sized clusters (see Section 4.1.1) allows such conditions to be realized that ensure the minimal contribution from fragmentation of different-sized clusters, interfering with the course of experiment (see Section 4.1.2).

4.1.1 Experiment and method. A schematic of the experimental setup is presented in Fig. 3 [124], and a detailed description of the nozzle design can be found in Ref. [163]. Sodium was put into a stainless steel furnace to be heated to 595 °C. The sodium vapor escaped through the nozzle (heated to 770 °C) together with the gas-carrier (argon) at a gas pressure of 7 atm above the nozzle. It was further passed through a skimmer cone to form a molecular/cluster beam where the cluster velocity was 1100 ± 30 m s^{-1} (for Na_{20}) [163]. The beam freely traversed a distance of 2.0 m and impinged on a circular Al diaphragm 3.175 mm in diameter that determined the lateral size of the fragmentating beam. After passing through the diaphragm, the beam was irradiated by a multimode argon ion laser. The laser beam intersected the cluster beam at a right angle. The mean photon energy of laser radiation was 2.5 eV. The laser beam was preliminarily expanded by a cylindrical lens and passed through an S slot 1 mm in width, ensuring uniform irradiation of the cluster beam in the transverse direction by a streak of light with an intensity of about 0.9 W mm^{-2}. At such an intensity, the Na_{20}-cluster signal detected decreased by approximately 30% due to cluster fragmentation.

Another circular A2 diaphragm 1.27 mm in diameter was placed behind the intersection region of the laser and cluster beams. The principle of the experiment is illustrated by Fig. 3. Photodissociation of the initial (mother) cluster results in the recoil of the daughter one and its deviation from the beam. However, if the daughter cluster formed near the aperture of the detector A2, it passes through the orifice and will be recorded by the detector. The probability of this process depends on the distance L from the cluster excitation zone to the diaphragm A2 and on the kinetic energy acquired by the daughter cluster during evaporation of an atom from the mother cluster [i.e., initial cluster temperature; see relation (3.1)].

Distance L between the laser spot and diaphragm A2 varied from 10 to 42 mm. Clusters having passed through A2 were ionized with filtered UV radiation from a Hg–Xe lamp.

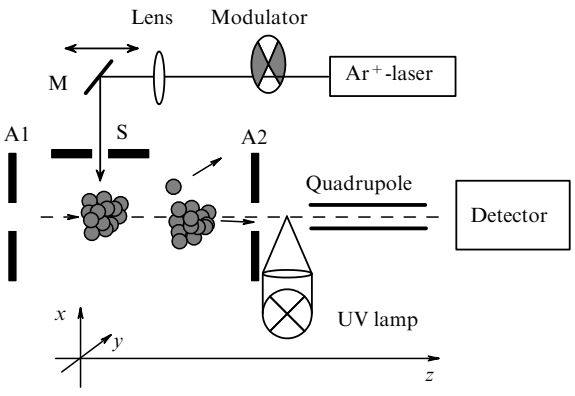

Figure 3. Layout of the experiment for determining sodium cluster temperature from the measurements of fragment recoil (escape from the beam) energy [124].

The filter served to retain short-wave UV radiation and let only photons with an energy close to the cluster ionization energy to pass in order to reduce the undesirable intense cluster fragmentation by UV radiation. The light from the UV lamp was focused on a spot measuring roughly 3 mm. Thereafter, the cluster ions were mass-selected with a quadrupole mass spectrometer and detected by a secondary electron multiplier. The results of the measurements were stored and processed on a personal computer. The signals induced by the cluster beam with and without laser excitation were recorded alternately by means of laser beam modulation with a 150-Hz chopper.

Once a photon is absorbed, the intensity of the signal from a given cluster, e.g., Na_{18}, changes as a result of two different reactions. One is Na_{18} fragmentation into smaller clusters, which occurs with probability α. A decrease in the signal caused by this process does not depend on the distance L. The other reaction is fragmentation of Na_{20} into Na_{18}, to which weight R^{-1} was attributed. The contribution from this process increases with decreasing L. Because the authors of paper [124] were interested in the channel in which the mother cluster Na_{20} dissociated into a daughter Na_{18} cluster, they normalized the measured signal of Na_{18} clusters as follows:

$$S_{18}(L) = R\,\frac{\mathrm{Na_{18}(laser\text{-}on)} - \mathrm{Na_{18}(laser\text{-}off)}\,\alpha}{\mathrm{Na_{20}(laser\text{-}off)} - \mathrm{Na_{20}(laser\text{-}on)}}\,. \qquad (4.1)$$

The two constants, R and α, were derived from the experimentally obtained signals. The former was found by normalizing the experimental data. The following procedure was used to determine the latter constant. For large distances L, the signal of Na_{18} clusters originating from Na_{20} clusters is proportional to the solid angle subtended by the A2 masking aperture of the detector and plotted from the point at which the mother cluster dissociates. In other words, the signal from the daughter Na_{18} cluster at large L is proportional to $1/L^2$. Due to this property, α is obtained from the dependence of the signal ratio Na_{18}(laser-on)/Na_{18}(laser-off) on $1/L^2$ by its linear extrapolation to $L = \infty$.

The fraction of mother Na_{20} clusters that undergo fragmentation after absorption of laser radiation must appear in the registration channels where daughter clusters are detected. The signal from Na_{20} clusters themselves does not practically change due to the fragmentation of larger clusters because the content of Na_{21}, Na_{22}, and Na_{23} clusters does not exceed 10% of Na_{20} (Fig. 4). The slope and curvature of experimental signal depletion curves, $S_N(L)$ (Fig. 5),

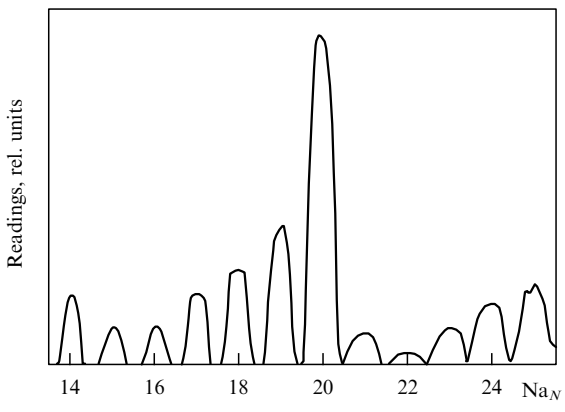

Figure 4. Typical mass spectrum of sodium clusters in the range from Na_{14} to Na_{25} [124].

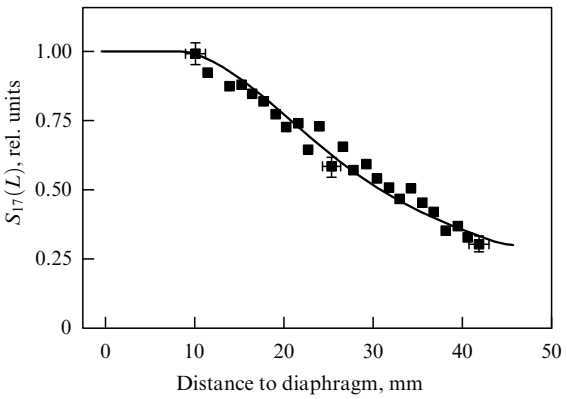

Figure 5. Na_{17} signal intensity measured as a function of distance from cluster excitation zone to detector diaphragm (squares) and the calculated curve for experimental data $T(Na_{20}) = 440$ K and evaporation channels (4.6) and (4.7) (solid line) [124].

depend on the recoil energy (and consequently temperature) of the daughter Na_N cluster.

The authors used the Weisskopf statistical theory [164, 165] for the kinetic analysis of cluster evaporation and treatment of the experimental data. Based on this theory, they constructed a model of cluster fragmentation and determined the temperature of the initial (mother) cluster and its fragments. The laser-heated clusters were cooled down due to the evaporation of monomers (Na) or dimers (Na_2). Calculations of cluster evaporation were made using the Monte Carlo method. Without going into particulars, here are the most important assumptions adopted and results obtained in Ref. [124].

To begin with, the authors took account of a decrease in the number of cluster's degrees of freedom after each evaporation step. The following relation should be satisfied for the case of monomer evaporation:

$$(3N-6)\,k_{\mathrm{B}}T_{\mathrm{m}} = \left\{\left[3(N-1)-6\right]+2\right\}k_{\mathrm{B}}T_{\mathrm{d}} + \Delta E_{\mathrm{ev}}\,, \qquad (4.2)$$

where T_{m} and T_{d} are the temperatures of the initial (mother) and daughter particles, respectively.

Thus, the authors made a standard assumption concerning temperature equilibrium between all vibrational degrees of freedom in a cluster. The difference between energies arising from the change in electronic degrees of freedom and free energies of the initial and daughter particles is contained in the dissociation or evaporation energy ΔE_{ev}. The additional term $2k_{\mathrm{B}}T_{\mathrm{d}}$ on the right-hand side of formula (4.2) takes account of the mean kinetic energy of an evaporated particle [165]. If the temperature of daughter clusters is measured in experiment, relation (4.2) can be used to determine the temperature of the mother cluster, bearing in mind that the evaporation energy (heat) ΔE_{ev} is known.

The relationship becomes somewhat more complex when a cluster loses a dimer via evaporation because the dimer has two rotational degrees of freedom, each with energy $k_{\mathrm{B}}T/2$, and one vibrational degree of freedom with energy $k_{\mathrm{B}}T$. Assuming that the dimer temperature is equal to the temperature of a daughter cluster, one obtains

$$(3N-6)\,k_{B}T_{\mathrm{m}} = \left\{\left[3(N-2)-6\right]+4\right\}k_{\mathrm{B}}T_{\mathrm{d}} + \Delta E_{\mathrm{ev}}\,. \qquad (4.3)$$

The authors of Ref. [124] determined the temperature of mother clusters prior to laser excitation using the following relation

$$(3N-6)\,k_{\mathrm{B}}T_{\mathrm{before}} + h\nu = (3N-6)\,k_{\mathrm{B}}T_{\mathrm{after}}\,, \qquad (4.4)$$

where $h\nu = 2.5$ eV is the energy of a laser radiation quantum.

4.1.2 The results of measurements. Figure 5 compares experimental and calculated data for the Na_{17} cluster. The measured signal being a function of daughter clusters recoil during evaporation of atoms or small fragments, it is necessary to take account of all possible fragmentation channels. For the case of an Na_{17} cluster giving a maximum signal in the experiments under consideration, the possible reaction channels for the formation of a given mass from the most widespread mass of Na_{20} clusters are the evaporation of monomers [relation (4.5)] or the evaporation of both monomers and dimers [relation (4.6)]. The evaporation of dimers from clusters with an odd number of electrons was not considered by the authors of Ref. [124] because such a process has never been observed in experiment [166]:

$$Na_{20} \rightarrow Na_{19} + Na \rightarrow Na_{18} + 2Na \rightarrow Na_{17} + 3Na, \qquad (4.5)$$

$$Na_{20} \rightarrow Na_{18} + Na_2 \rightarrow Na_{17} + Na + Na_2\,. \qquad (4.6)$$

An additional contribution may come from Na_{19} cluster fragmentation [see relation (4.7)]. However, it may be nothing other than a small correction, since the content of Na_{20} is almost 4 times that of Na_{19} (see Fig. 4). Nevertheless, the authors took account of this process as well:

$$Na_{19} \rightarrow Na_{18} + Na \rightarrow Na_{17} + 2Na\,. \qquad (4.7)$$

The above reactions include all channels for the formation of the product being detected, Na_{17}. Indeed, the fragments of Na_{18} dissociation are so hot [124] that they continue to decay till they reach the detector. On the other hand, evaporation channels of clusters larger than Na_{20} will be efficiently closed before the mass of Na_{17} is achieved.

These fragmentation channels were used in Ref. [124] to fit experimental and theoretical data. As a result, two temperature variants were obtained. Channel (4.5) gives the following sequence of temperatures for the fragments: $T(Na_{19}) = 865$ K, $T(Na_{18}) = 685$ K, and $T(Na_{17}) = 480$ K. Then, the temperature of the mother Na_{20} cluster is 515 K prior to its laser excitation. In the second option [relation (4.6)], the temperatures are $T(Na_{18}) = 780$ K and $T(Na_{17}) = 575$ K, respectively. In this case, the temperature of the mother Na_{20} cluster prior to excitation reaches 440 K. Additional measurements and analysis of the data obtained in Ref. [124] showed that dissociation channel (4.6) makes up the main one for the production of Na_{17} fragments. The authors also considered the sources of measurement and calculation errors and found their limiting value to be ± 65 K. Thus, the temperature of Na_{20} clusters in a beam is $T(Na_{20}) = 440 \pm 65$ K. For comparison, the nozzle temperature of the cluster beam source was 1040 K.

4.1.3 Conclusions. To sum up, the measurement of the temperature of free metallic Na_{20} clusters in a beam [124] is based on their excitation by laser radiation. Absorption of laser photons heated the clusters and thereby induced a sequence of their fragmentations during which the clusters successively evaporated atoms and dimers and cooled down. The kinetic energy released in the course of cluster evaporation was measured from the recoil of daughter fragments. The temperatures of Na_{20} clusters obtained by the authors were in excellent agreement with those calculated in the framework of the evaporative ensemble model [124].

The rather complicated experiments on the measurement of Na_{20} cluster temperature in a molecular beam described in the preceding paragraphs could be conducted only because this cluster is the dominant magic cluster and its content is much greater than that of the nearest similar-sized sodium clusters in the same beam. It is this finding that made it possible to detect fragmentation channels of the mother cluster and pathways for the formation of daughter clusters, and also to accurately measure the fraction of daughter clusters produced upon dissociation (evaporation) of the mother Na_{20} cluster. Therefore, this experiment demonstrates how difficult it is to choose the method for measuring cluster temperature and the conditions under which determination of free cluster temperature in molecular beams becomes possible.

4.2 Determination of the temperature of excited $(CF_3I)_N$ clusters from measurements of the kinetic energy of dissociation fragments (CF_3I molecules)

In this and the next sections, we shall deal with the kinetic methods for measuring the temperature of free molecular van der Waals clusters in beams that have been recently developed at the Institute of Spectroscopy, Russian Academy of Sciences (Troitsk). To begin with, we shall consider the method for determining the temperature of $(CF_3I)_N$ clusters (with the mean number of particles $N \approx 110$) in a molecular beam by direct measurement of the kinetic energy of dissociation products, i.e., CF_3I molecules [167]. The cluster fragmentation was induced by intense IR radiation from a pulsed CO_2 laser. CF_3I molecules making up $(CF_3I)_N$ clusters are easy to excite by CO_2-laser resonance radiation (including multiphoton excitation [168, 169]) affecting the vibration ν_1 (1075 cm^{-1}) [170] of the molecules. The processes of IR multiphoton excitation (MPE) and multiphoton dissociation (MPD) of these molecules are fairly well known [171], including those in molecular beams and jets [172–176]. As reported in an earlier study [177], CF_3I molecules readily arrange themselves into clusters during ultrasonic gas expansion through a pulsed nozzle. The main characteristics of the resulting beam of $(CF_3I)_N$ clusters were measured. Moreover, it was shown that a CO_2-laser pulse induces dissociation of these clusters. A method for the detection of $(CF_3I)_N$ clusters was developed based on multiphoton particle ionization by UV radiation (UV-MPI) [177]. Conditions for the detection of CF_3I molecules themselves by UV-MPI were elucidated in the work being considered [167]. In other words, the selective detection of both initial clusters and their decay products, CF_3I molecules, became possible. It enabled the authors of Ref. [167] to measure the concentration of clusters and molecules in a beam both before and after their excitation by IR laser pulses. In this way, the kinetic energy of CF_3I molecules resulting from $(CF_3I)_N$ cluster decay was measured.

4.2.1 The experimental setup and the measurement method. The experimental setup (Fig. 6) is described in detail in papers [167, 178]. $(CF_3I)_N$ clusters were generated by gasdynamic cooling of a $CF_3I + Ar$ mixture (with a pressure ratio over the

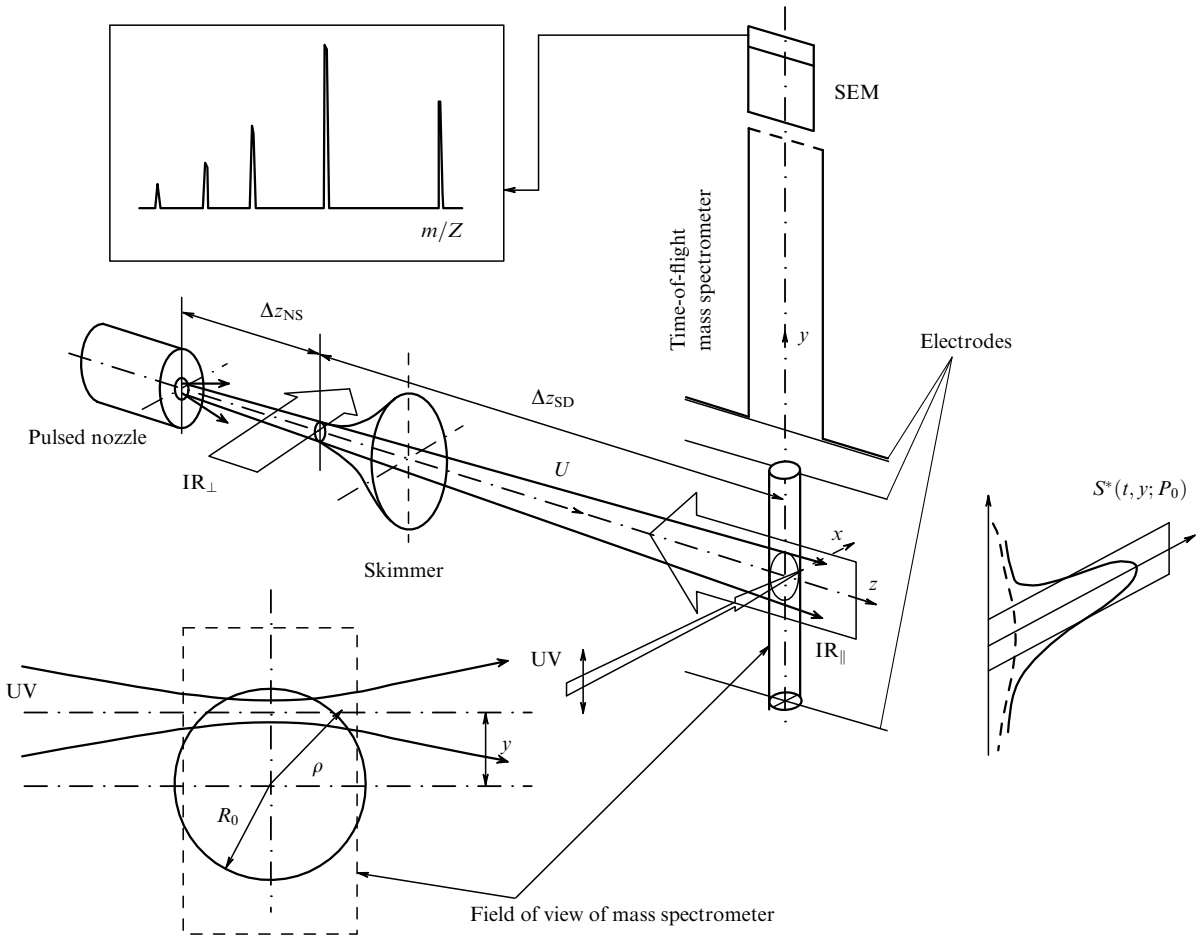

Figure 6. Elements of the experimental setup for measuring $(CF_3I)_N$ cluster temperature (m — ion mass, Z — degree of ionization, P_0 — pressure above the nozzle, and U — mean translational velocity) [167].

nozzle reaching 1 : 5) during supersonic gas expansion through a General Valve type pulsed nozzle with the orifice diameter $D_{noz} = 0.8$ mm and nozzle-opening pulse duration ca 300 μs. The gas pressure above the nozzle varied in the range of $P_0 = 0-5$ atm. A skimmer placed at a distance of $\Delta z_{NS} = 38.5$ mm from the nozzle had the intake orifice diameter $D_S = 0.66$ mm and was used to cut a molecular/cluster beam. The particle beam entered the chamber of the time-of-fight mass spectrometer (TOFMS). At a distance of $\Delta z_{SD} = 96.5$ mm from the skimmer intake orifice, the cluster beam intersected the mutually perpendicular axes of the mass spectrometer and the beam of focused (lens focal distance $f = 12$ cm) UV-laser light (second harmonic of the Xe-Cl laser-pumped dye laser; tuning range of $\lambda = 210-260$ nm; pulse duration 10 ns) used for UV-MPI of the clusters. The pulsed CO_2 laser was utilized for vibrational excitation and IR photodissociation of $(CF_3I)_N$ clusters. The half-height pulse duration was around 150 ns. Particles could be IR-excited either before they passed through the skimmer (in this case, the laser beam crossed the cluster beam) or in the TOFMS chamber at the intersection of the UV radiation beam and the TOFMS axis (see Fig. 6). In the latter case, the radiation from the CO_2 laser was directed oppositely and at a small angle to the cluster beam. The synchronizing system employed in the experiment ensured the desired synchronization of all the pulses.

The area of the UV radiation spot (at the $1/e$ level) at the lens focus on the TOFMS axis was ~ 0.013 mm^2, and the pulse energy was below 60 μJ. Parallel displacement of the probe UV radiation along the TOFMS axis made it possible to measure the transverse profile of the cluster beam (see Fig. 6). The length of the cluster beam pulse in the UV probing region was about 500 μs. Particle ionization was effected approximately in the middle of this pulse. The resulting ions were detected in TOFMS equipped with a secondary-electron multiplier (SEM). Ion signals from the SEM, as well as IR and UV pulse energies were recorded by a digital oscillograph and loaded into a computer to be stored and processed.

4.2.2 UV-MPI of $(CF_3I)_N$ clusters and CF_3I molecules. As mentioned above, the authors of Ref. [177] explored UV-MPI of $(CF_3I)_N$ clusters using an excimer XeCl laser ($\lambda = 308$ nm). The mass spectrum exhibited only peaks of I^+ and I_2^+ ions. It was concluded that I_2^+ is a product of $(CF_3I)_N$ cluster ionization resulting from intracluster reactions, which permits using this peak for the selective detection of the clusters of interest. Ion signals from free CF_3I molecules under conditions of Ref. [177] were negligibly small. Therefore, the authors of Ref. [167] preliminarily studied photoionization of CF_3I clusters and molecules using a tunable source of UV radiation. Tuning of exciting UV radiation to a shorter-wavelength region gave evidence of the presence of CF_3^+ ion peaks comparable with I^+ and I_2^+ peaks in terms of intensity. Typical mass spectra obtained after UV-MPI of CF_3I clusters and free molecules at 230 nm are shown in Fig. 7. This

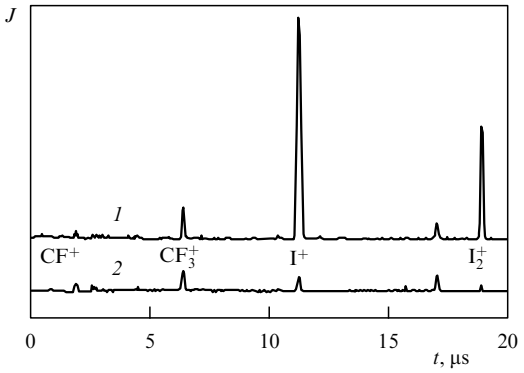

Figure 7. Time-of-flight photoionization mass spectra: *1* — cluster beam; *2* — free CF_3I molecules (after roughly 98% IR dissociation of $(CF_3I)_N$ clusters); $\lambda = 230$ nm, and $E_{UV} = 50$ μJ [167].

wavelength was utilized in work [167] for further measurements.

In the case of a cluster beam, the mass spectrum (spectrum *1* in Fig. 7) is characterized by the I_2^+ peak ($m/Z = 254$) and the accompanying more intense I^+ peak ($m/Z = 127$). The measured dependence of the signal on the UV radiation flux energy density Φ_{UV} for I_2^+ ion has the form $S_{254}(\Phi_{UV}) \propto \Phi_{UV}^{0.72}$; for I^+, the exponent is greater by almost unity: $S_{127}(\Phi_{UV}) \propto \Phi_{UV}^{1.77}$. If the ionization potential of $(CF_3I)_N$ clusters is not significantly different from that of CF_3I molecules (IP = 10.37 eV [179] — ionization potential of a molecule), two quanta of radiation at $\lambda = 230$ nm are sufficient to ionize these clusters. The proximity of the exponent to unity in the dependence $S_{254}(\Phi_{UV})$ appears to be related to the saturation of the process due to one-photon resonance with the A-band in CF_3I (see paper [180] for the diagram of CF_3I energy levels). As for I^+ ions, they are likely to form in I_2^+ dissociation. Figure 7 shows a peak of CF_3^+ ions ($m/Z = 69$) in the mass spectrum characterized by the dependence $S_{69}(\Phi_{UV}) \propto \Phi_{UV}^{2.25-2.5}$, suggesting the multiphoton character of its formation.

As regards free CF_3I molecules, the main products of their photoionization at 230 nm are CF^+ ($m/Z = 31$), CF_3^+ ($m/Z = 69$) giving the highest peak at room temperature, I^+ ($m/Z = 127$), and CF_3I^+ ($m/Z = 196$) (under specific conditions). The dependences of ion signals from CF_3^+ and I^+ on energy density Φ_{UV} have a power-like character with roughly identical exponents equal to 2.2, i.e., $S \propto \Phi_{UV}^{2.2}$. The dependence $S(\Phi_{UV})$ for CF_3I^+ is almost linear. It was shown in paper [167] that the yields of CF^+ and I^+ ions depend on the vibrational energy of CF_3I molecules. In the case of multiphoton IR excitation of CF_3I molecules, the yield of CF^+ and I^+ ions rapidly grows with energy density Φ_{IR} ($S \propto \exp(\Phi_{IR})$) up to the values comparable with the threshold energy density Φ_{th} for molecular dissociation. As Φ_{th} is surpassed, signals from these ions start to decrease due to the decay of the initial molecules (products of IR dissociation of the molecules themselves, i.e., CF_3 and I in the ground electronic states, yield no ions under the conditions of these experiments). At the same time, measurements showed that the signal of a CF_3^+ ion only weakly depends on the degree of vibrational molecular excitation, although it starts to decrease at excitation levels above the molecular dissociation threshold. Such a behavior of the CF_3^+ signal is of importance when it is used for the diagnostics of free molecules formed as a result of IR dissociation of the clusters, because the signal amplitude depends first and foremost on the number of newly formed molecules and is unrelated to their internal state.

The difference between photoionization mass spectra of cluster beams and free molecules is quite apparent in Fig. 7 from a comparison of spectrum *1* taken before the cluster beam excitation and spectrum *2* recorded immediately after cessation of the radiation pulse from the CO_2 laser. These mass spectra were obtained after almost complete (close to 100%) beam clusterization in the detection area. At $\Phi_{IR} = 0.08$ J cm^{-2}, the cluster constituent of the beam virtually decays (98% depletion of the I_2^+ signal), whereas the CF_3^+ signal present in both spectra is depleted by only 25%. Bearing in mind that the total number of molecules in the detection area does not change during the pulse propagation time (as will be discussed below) due to the low expansion velocity of free molecules, the comparison of the signals from the cluster constituent and the free molecules gives the relative efficiency of CF_3^+ ionization yield in these two cases. Then, the signal from CF_3^+ can be distinguished based on the knowledge of the behavior of molecules in the cluster constituent obtained from the measurement of the I_2^+ signal. The former signal corresponds to that of free molecules at any (not only 100%) cluster dissociation. It is this approach that was used in work [167] to measure cluster decay kinetics and the rate of production of decay products.

4.2.3 Dissociation of $(CF_3I)_N$ clusters by IR laser radiation. IR excitation and dissociation of clusters in Ref. [167] were induced by affecting CF_3I vibration ν_1 on the 9R (14) line (1052.2 cm^{-1}) with CO_2-laser radiation in the region of $(CF_3I)_N$ absorption maximum [177]. The transverse size of the laser beam (see Fig. 6, $IR_{||}$ longitudinal geometry) was much greater than the cluster beam diameter, which accounted for the presence of clusters undergoing excitation in a practically uniform laser radiation field. Measurements of two types were made. First, the authors measured the signal S_{254} from I_2^+ ions depending on flux energy density Φ_{IR} of IR radiation immediately after cessation of the laser pulse. Second, they measured signal variation in time, $S_{254}(t)$, including the propagation time of the IR pulse itself.

Figure 8 depicts the characteristic dependence $S_{254}(\Phi_{IR})$ for $P_0 = 1.15$ atm, corresponding to the cluster size $N \approx 110$ [167]. Rapid signal depletion with the growth in Φ_{IR} unambiguously suggests cluster dissociation (decay), with the effective dissociation occurring at Φ_{IR} values much smaller than the threshold energy density for the multi-

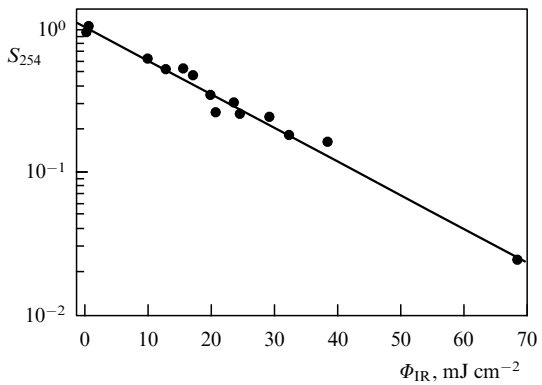

Figure 8. The dependence of normalized ion signal S_{254} from $(CF_3I)_N$ clusters on IR radiation energy density Φ_{IR}; $P_0(CF_3I + Ar) = 1.15$ atm, and $N \approx 110$ [167].

photon IR dissociation of free molecules. The measured dependence of I_2^+ signals on energy density per pulse is fairly well described by an exponential function in the form $S_{254}(\Phi_{IR}) = S_{254}^0 \exp(-k\Phi_{IR})$ (solid line in Fig. 8). An analogous exponential form of the dependence of the $(CF_3I)_N$ IR-photodissociation yield on Φ_{IR} was reported earlier in Refs [177, 181]. Such behavior is characteristic of a process in which a rise in the cluster internal energy E due to radiation absorption with increasing Φ_{IR} ($\Delta E = \sigma n \Delta\Phi_{IR}$, σ is the IR absorption cross section) above the threshold energy density for dissociation results in the detachment of a part (ΔN) of the molecules from the cluster and corresponding expenditure of the excess energy on accomplishing this process ($\Delta E = -\varepsilon_0 \Delta N$, ε_0 is the molecular bond energy in the cluster). Then, the number of molecules remaining inside the cluster is given by

$$N = N_0 \exp\left(-\frac{\sigma}{\varepsilon_0}\,\Phi_{IR}\right). \tag{4.8}$$

If the photoionization efficiency ζ depends on the cluster size and this size effect has a power-like character, $\xi(N) \propto N^g$, then (taking account of cluster size changes during dissociation) the behaviour of the corresponding cluster signal will have the same exponential form for clusters [177]:

$$S_{254} = S_{254}^0 \exp\left[-(1+g)\,\frac{\sigma}{\varepsilon_0}\,\Phi_{IR}\right] = S_{254}^0 \exp(-k\Phi_{IR}), \tag{4.9}$$

where k is the parameter depending on concrete excitation and ionization conditions for clusters [167].

It should be noted that the parameter k may be significantly different in experiments with one and the same cluster system using different sources of IR and/or UV radiation [167] due to both the difference in IR absorption cross sections $\sigma(\nu_{IR})$ and the size effect influencing the photoionization efficiency $\xi(N; \nu_{UV})$. By analyzing the results of studies [167, 177], the authors arrived at the conclusion that the size effect for the multiphoton ionization of $(CF_3I)_N$ clusters by 230-nm UV radiation can be neglected and signal S_{254} assumed to be directly proportional to the number of CF_3I molecules condensed into clusters.

4.2.4 Determining the temperature of $(CF_3I)_N$ clusters. Using the method for the detection of free CF_3I molecules from the signal S_{69} of CF_3^+ ions, developed in Ref. [167] and described in Sections 4.2.1–4.2.3, it is possible to trace the kinetics of the formation and subsequent evolution of these molecules in the course of $(CF_3I)_N$ fragmentation under the effect of IR laser pulses. The typical temporal evolution of the signal S_{69} from free CF_3I molecules is shown in Fig. 9. It can be seen that the signal grows during the laser pulse at a rate similar to the cluster dissociation rate (calculated dashed line in Fig. 9). At a certain moment, it begins to decrease as a result of scattering of newly formed molecules from the cluster dissociation area. Comparing the measured spatial–temporal evolution of the signal S_{69} and the corresponding model, one can deduce the mean velocity and respective kinetic energy (translational temperature) of the free CF_3I molecules generated by cluster dissociation, and, consequently, the temperature of the excited $(CF_3I)_N$ clusters.

The ion signal $S(t, y)$ recorded in the experiment at an instant of time t depends on density D, the form of transverse distribution $B_\perp(t, \rho)$ of the particles being probed, and the ionization efficiency $\xi(I(\mathbf{r}))$, $\mathbf{r} = (x, y, z)$. The last parameter

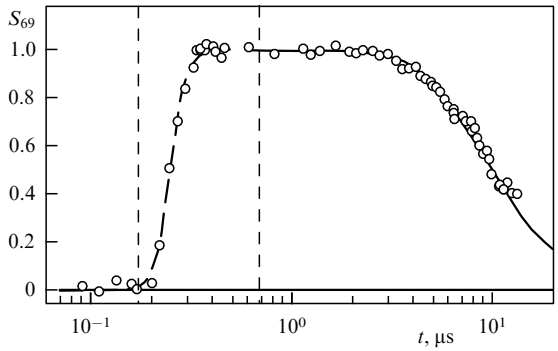

Figure 9. Normalized ion signal $S_{69}(t)$ from free CF_3I molecules at $\Phi_{IR} = 67.45$ mJ cm^{-2}. Dashed curve — calculation for $\tau = 1$ ns (see the text); solid curve — simulated behavior of the signal $S_{69}(t, y = 0)$ for $t > t_1$ at the fitted value of $V_{M\perp} = 127$ m s^{-1}. Duration of the exciting IR laser pulse is bounded by vertical dashed lines [167].

should take account of spatial inhomogeneity of the ionizing radiation beam in the observation volume V_{obs} depending on the field of view of the mass spectrometer (see Fig. 6). In other words, the signal being detected is given by the following expression [167]:

$$S(t, y) \propto \iiint_{V_{obs}} DB_\perp(t, \rho)\, \xi(I(\mathbf{r}))\, \mathrm{d}v. \tag{4.10}$$

Here, $B_\perp(t, \rho)$ is the normalized function describing the transverse distribution pattern (along coordinate ρ; see Fig. 6) of the particles in the working area of the mass spectrometer. Its form depends on the conditions under which the particles flow out of the nozzle (nozzle design, temperature, pressure, and gas composition), and reflects variations in the particle transverse distribution attributable to beam spreading governed by the transverse component $V_\perp$ of the velocity of the chaotic (thermal) motion of beam particles. The role of this factor in cluster beam formation was discussed in detail in Refs [180, 182]. The simplest description of particle motion is possible when the system of particles is characterized by an integrated parameter, such as the most probable velocity $V_\perp$ of chaotic motion. Let the transverse spatial distribution of the beam immediately after it passes the skimmer have a rectangular profile, and the subsequent free particle motion in the space behind the skimmer obey [167] the Maxwell ellipsoid drift distribution over velocities v:

$$f(v) \propto \left(\frac{1}{\sqrt{\pi} V_\parallel}\right) \exp\left(\frac{-(v_\parallel - U)^2}{V_\parallel^2}\right)\left(\frac{1}{\pi V_\perp^2}\right) \times \exp\left(\frac{-v_\perp^2}{V_\perp^2}\right), \tag{4.11}$$

where U is the velocity of the beam directional motion, and $V_\parallel$ and $V_\perp$ are the longitudinal and transverse components, respectively, of the most probable velocity of the chaotic motion of particles in the beam. In this case, the transverse beam distribution in the detection area takes the form [180]

$$B(\Delta t, \rho, V_\perp) = \frac{1}{\pi \Delta t^2 V_\perp^2} \times \left[\int_0^{2\pi}\left(\int_0^{R_0} r \exp\left(\frac{-(\rho^2 + r^2 - 2r\rho\cos(\varphi))}{\Delta t^2 V_\perp^2}\right)\mathrm{d}r\right)\mathrm{d}\varphi\right], \tag{4.12}$$

where $R_0 = D_S(\Delta z_{NS} + \Delta z_{SD})/(2\Delta z_{NS}) = 1.15$ mm is the geometric radius of the beam in the ionization area, Δz_{NS} is the distance from the source to the skimmer, Δz_{SD} is the distance between the skimmer and the ionization area, D_S is the diameter of the skimmer, and $\Delta t = \Delta z_{SD}/U$ is the time of flight from the skimmer to the ionization area (see Fig. 6). The time of flight Δt was determined from the arrival time of the IR-photodissociation label generated at the skimmer input in an experiment with perpendicular geometry ($IR_\perp$; see Fig. 6) (see Ref. [180] for details). A comparison of experimental $S^*(t, y)$ and theoretical $S(t, y)$ signal amplitudes corresponding to the transverse particle distribution at instant t gives the transverse component $V_{cl\perp}$ of the most probable cluster velocity in the beam and the transverse distribution density $B(\rho)$ of clusters at the moment of IR excitation of the beam. In the experiments reported in paper [167] ($N \approx 110$), the most probable transverse cluster velocity $V_{cl\perp}$ in the beam was estimated at 1.1 m s^{-1}.

As shown experimentally in paper [167], cluster dissociation producing free molecules occurred during an IR laser pulse. The spatial distribution density of CF_3I molecules formed up to the instant of pulse cessation t_1 was close to the starting particle distribution in the cluster beam. However, the additional kinetic energy acquired by the molecules in cluster decays caused them to spread. As a result, their density in the central part of the beam decreased; it influenced the behavior of the corresponding signals specially on the beam axis [($S(t, y=0)$; see Fig. 9]. The most probable molecular velocity $V_{M\perp}$ can be determined based on the above model considerations. However, it requires that the 'prehistory' be somewhat changed so that simulation starting (at moment t_0) from the original rectangular profile of the transverse distribution and the fitting velocity parameter $V_{M\perp}$ gives, after the span of time $\Delta t = t_1 - t_0$, the distribution profile $B_\perp(t_1 - t_0, \rho; V_{M\perp})$ for which the behavior of the calculated signal $S(t_1, y)$ coincides with that of the experimental signal at the IR-pulse cessation instant t_1. In this case, the behavior of distribution $B_\perp(t - t_0, \rho; V_{M\perp})$ and the corresponding model signal $S(t, y = 0)$ at any time thereafter ($t > t_1$) must also correspond to the experimental one. This situation is illustrated by Fig. 10 showing the starting rectangular distribution at instant of time t_0 and the experimental behavior (marks in curve *2*) of signal $S^*(t_1, y)$ at instant t_1 (the transverse beam profile was obtained by scanning UV radiation along the y-axis; see Fig. 6). Solid curve *2* drawn through the experimental points in Fig. 10 is a result of model analysis. The figure also demonstrates the behavior of theoretical (curve *1*) and measured (marks) signals from CF_3I molecules on the beam axis, $S(t, y = 0)$, at the fitted value of $V_{M\perp} = 127$ m s^{-1}. The agreement is rather good. The velocity value obtained corresponds to the translational temperature of CF_3I molecules, $T_{tr} = 185$ K, while the internal temperature of $(CF_3I)_N$ clusters with $N \approx 110$ only slightly differs from this value (by no more than 10–20%) [167].

4.2.5 The dependence of $(CF_3I)_N$ cluster temperature on the exciting IR pulse energy density. The authors of work [167] considered the dependence of $(CF_3I)_N$ cluster temperature on the exciting IR laser pulse energy density, based on the measurements of the kinetic energy of CF_3I molecules. The $V_{M\perp}$ values measured during variation of Φ_{IR} in the range from 10 to 75 mJ cm^{-2} are presented in Fig. 11a. Figure 11b depicts the dependence of cluster dissociation yield β on Φ_{IR}

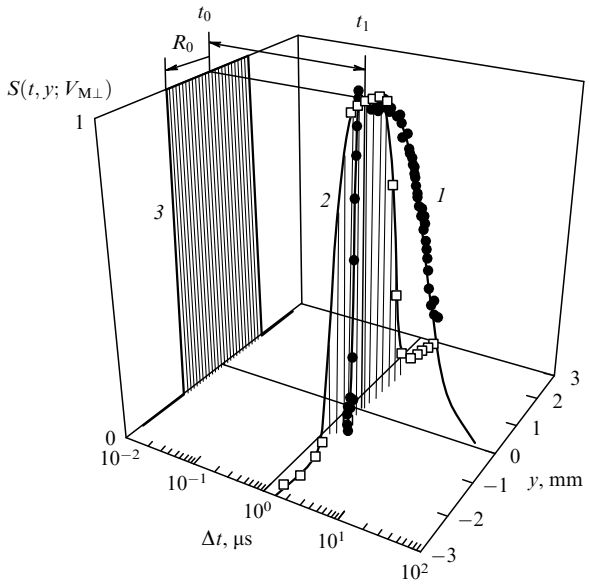

Figure 10. Spatial–temporal evolution of the ion signal $S_{69}(t, y)$ from free CF_3I molecules: *1* — time dependence of the ion signal $S_{69}(t, y = 0)$ on the beam axis [• — experiment for $\Phi_{IR} = 67.45$ mJ cm^{-2}; the curve — model calculation ($V_{M\perp} = 127$ m s^{-1})]; *2* — transverse distribution of the ion signal $S_{69}(t = t_1, y)$ along the y-axis (see Fig. 1) at instant t_1 of the cessation of the IR pulse (□ — experiment for $\Phi_{IR} = 67.45$ mJ cm^{-2}; the curve — model calculation); *3* — the starting model distribution evolving for time $\Delta t = t_1 - t_0$ into the distribution for which the behavior of the model signal $S_{69}(t = t_1, y)$ coincides with experiment (curve 2) [167].

derived from the data given in Fig. 8. (Parameter β defines a fraction of clusterized molecules that left clusters after IR irradiation with the flux energy density Φ_{IR}.) From this figure we notice that there is a segment corresponding to the initial increase in the velocity of outgoing molecules: the value of $V_{M\perp}$ grows from 110 to 135 m s^{-1} with increasing Φ_{IR} from 10 to 35 mJ cm^{-2}, and the dissociation yield amounts to $\beta = 80\%$. This change in $V_{M\perp}$ corresponds to a change in temperature T_{tr} of translational degrees of freedom of CF_3I molecules from 140 to 215 K.

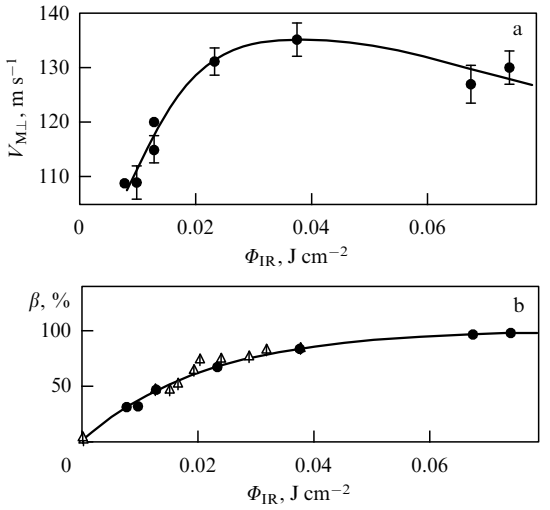

Figure 11. (a) Expansion velocity $V_{M\perp}$ of free CF_3I molecules, and (b) cluster dissociation yield β plotted as functions of energy flux density of the passed IR pulse; $P_0(CF_3I + Ar) = 1.15$ atm, and $N \approx 110$ [167].

The dissociation yield continues to grow with a further increase in Φ_{IR}, but the velocity of the outgoing molecules and their temperature begin to decrease. According to the authors of Ref. [167], such a behavior of the velocity of CF_3I molecules formed in cluster dissociation depending on Φ_{IR} is due to at least two causes. The main cause of the initial rise in T_{tr} is related to the competition between IR excitation and subsequent evaporation of the clusters. In the approximation of a quasistationary regime, an increase in the rate of radiative excitation (with growing Φ_{IR}) leads to an increase in the evaporation rate, the temperature of $(CF_3I)_N$ clusters, and, accordingly, T_{tr}. The size effect may be responsible for the descending velocity of molecules leaving the cluster surface at high excitation energy densities. As is known [1, 39], the bond energy (evaporation heat) in clusters depends on their size and begins to decrease upon transition to the region of relatively small clusters. It was shown in Ref. [183] that the evaporation heat ΔE_{ev} for certain molecular clusters varies but insignificantly in the range of $N \approx 30-1000$ and begins to sharply decrease at smaller cluster sizes (see also reviews [35, 39]). The estimates made in paper [167] suggest that the mean size of $(CF_3I)_N$ clusters prior to irradiation amounted to $N \approx 110$. This means that the value of N at $\beta = 80\%$ falls to $N \approx 20$, i.e., into the region where ΔE_{ev} begins to markedly decrease. The authors argued that it is this effect that is first and foremost responsible for the experimentally examined fall in T_{tr} (consequently, in cluster temperature as well) in the region of large β (Fig. 11a, b).

4.3 The probe method for measuring the temperature of large $(CO_2)_N$ clusters (nanoparticles) in a cluster beam

4.3.1 The essence of the method and experiment. A universal probe method for measuring the temperature of clusters and nanoparticles in molecular beams has been developed recently [184, 185]. It utilizes molecules (or atoms) as a probe thermometer to measure the temperature of clusters (nanoparticles). A molecule is captured by a cluster in crossed molecular and cluster beams and sublimes (evaporates) after thermalization with it from the cluster surface, carrying information on the cluster velocity and temperature. The kinetic and internal energies (quantum state) of the molecule serve as a measure of cluster temperature. The method is essentially analogous to that for measuring cluster temperature from the kinetic energy of taking-off fragments [124, 125, 167] (see also Section 4.2). However, it requires neither excitation of clusters nor induction of their fragmentation. Moreover, a variety of atoms and molecules suitable for detection can be used as a probe thermometer to measure the temperature of a cluster or nanoparticle that differ from those forming the cluster itself. The method is realized if the bond energy of monomers in the cluster exceeds the coupling energy between cluster and probe molecules. This condition satisfied, trapped molecules rather than cluster molecules (atoms) are very likely to sublime (evaporate) from the surface of the cluster without its excitation.

The said constraint is fulfilled for many clusters and molecules (atoms) and was employed in Refs [184, 185], where the temperature of large van der Waals $(CO_2)_N$ ($N \geqslant 100$) clusters (nanoparticles) in a cluster beam was measured using SF_6 molecules as tiny probe thermometers. The sublimation heat (energy) of SF_6 (5.46 kcal mol^{-1} [186]) is lower than that of CO_2 (6.03 kcal mol^{-1}[186]). The probability of sublimation (evaporation) of the trapped molecules from the cluster surface increases because they transfer their energy to the cluster, thus raising its temperature [28, 117, 187, 188]. In order to determine cluster temperature by the proposed method, it is necessary to measure either the kinetic or the internal energy of the molecules sublimating from the cluster surface. However, in certain cases (e.g. SF_6) the vibrational and rotational temperatures (internal energy) of the molecules can be estimated from the spectra of IR multiphoton absorption (MPA) [189–191].

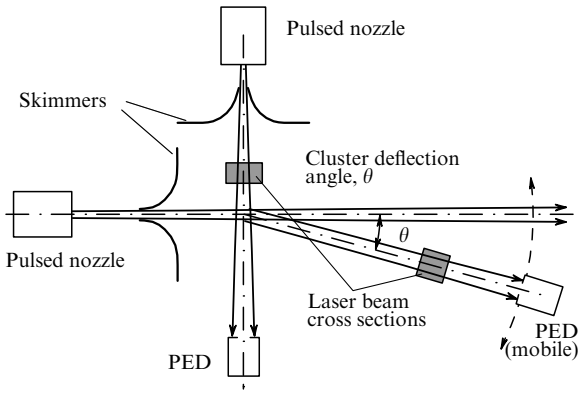

Figure 12. Schematic of an experiment with the use of the probe method for measuring the temperature of clusters (nanoparticles) in a beam. Molecules are captured by the clusters from the crossing molecular beam and after a time sublime from the cluster surface, carrying information about cluster velocity and temperature [184].

The essence of the method and experimental procedure is clarified in Fig. 12. An intense pulsed $(CO_2)_N$ cluster beam intersects a pulsed SF_6 molecular beam at a right angle. SF_6 molecules are captured by $(CO_2)_N$ clusters in the beam intersection region. As the molecules transfer a momentum to the clusters [28, 187, 188], the latters become deflected at a certain angle. The cluster beam was generated by passing through a pulsed 'current loop' type nozzle [192] with an opening diameter of 0.75 mm and an opening pulse time (FWHM) of 120 μs. The gas pressure above the nozzle varied between 0.5 and 4.5 atm. The nozzle was cut in the shape of a cone with a whole conical angle of 26°, and the length of the cone measured 30 mm. An in-depth study of cluster formation in a pulsed nozzle was reported in paper [193]. In the experiment being considered, $(CO_2)_N$ clusters were composed of $N \geqslant 10^2-10^3$ particles. Note that such large clusters have a crystalline structure [35, 105, 106].

The SF_6 molecular beam was produced in a pulsed General Valve type nozzle (electromagnetic valve) with an orifice 0.8 mm in diameter. The opening pulse duration (FWHM) was about 300 μs. The gas pressure above the nozzle varied from 0.5 to 2.5 atm. The cluster and molecular beams were extracted from the pulsed jets (generated with the aid of such nozzles) taking advantage of conical diaphragms (skimmers) having intake orifices 3 and 6 mm in diameter, respectively, which were placed at a distance of 30 and 26 mm from the nozzles. The molecular and cluster beams were detected by uncooled pyroelectric detectors (PEDs) having a temporal resolution of about 5–10 μs [189, 191]. The detectors were placed at various distances from the nozzles. The distances between the nozzle and the center of the beam intersection region were 93 and 90 mm for the cluster and molecular beams, respectively. The vacuum chamber for beam generation was pumped down to a pressure of $\approx 3 \times 10^{-6}$ Torr using a diffusion pump.

Vibrational excitation of SF_6 molecules was effected by intense ($\geqslant 10^6-10^7$ W cm^{-2}) frequency-tuned radiation of a pulsed CO_2 laser. The pulse energy reached 3 J, with the pulse duration (FWHM) of around 100 ns. Active molecular vibration ν_3 was excited in the IR region (948 cm^{-1} [194]). The laser beam intersected the molecular one at a right angle at a distance of 75 mm from the nozzle cut (see Fig. 12). When studying IR-MPA of SF_6 molecules sublimated from the surface of $(CO_2)_N$ clusters, they were excited at a distance of 23 mm from the beam intersection region where the laser spot was approximately 10×10 mm. Studies of the IR-MPA of SF_6 molecules in the molecular beam and SF_6 molecules sublimated from the cluster surface were carried out with the use of a pyroelectric detection of the absorbed energy [168, 169, 189, 191]. The signal induced on a PED by a cluster beam and sublimated molecules was amplified (amplification coefficient ca 100) and fed into a Tektronix TDS-1002 digital oscillograph. Both molecular and cluster beams operated in the single-pulse mode. PED readings were averaged over 16 pulses.

The cluster deflection angle resulting from the capture of molecules is given by the relation

$$\tan\theta = \frac{\sin\alpha}{m_1 v_1/m_2 v_2 + \cos\alpha}\,, \tag{4.13}$$

where m_1, m_2 and v_1, v_2 are the masses and velocities of clusters and molecules, respectively, and α is the angle between the cluster and molecular beams. Under experimental conditions ($\alpha = 90°$, $m_2 \approx 146$ a.m.u., $v_1 \approx 450$ m s^{-1}, and $v_2 \approx 430$ m s^{-1} are the measured velocities of clusters and molecules in the beams), $(CO_2)_N$ clusters containing $N = 100$ particles that captured separate SF_6 molecules were deflected through the angle $\theta \approx 1.8°$, and those with $N = 1000$ particles through the angle $\theta \approx 0.18°$.

As revealed in Ref. [195], SF_6 molecules trapped by clusters sublimated after a time from their surfaces. The authors arrived at this inference based on examining the signal induced by vibrationally excited SF_6 molecules on the detector recording cluster beams, and on the shape of the time-of-flight spectra of the $(CO_2)_N$ cluster beam obtained with and without the assistance of a molecular beam. In the laboratory coordinate system, molecules sublimating from the cluster surface move largely along the cluster beam and induce an additional signal on the detector (Fig. 13a, b).

The lifetime τ of an SF_6 molecule captured on the $(CO_2)_N$ cluster surface depends on the molecular sublimation (evaporation) energy and cluster temperature; it can be estimated from the expression [196]

$$\tau = \tau_0 \exp\left(\frac{\Delta E_{ev}}{k_B T_{cl}}\right), \tag{4.14}$$

where τ_0 is the vibrational period of the molecule on the cluster surface with respect to the van der Waals bond, ΔE_{ev} is the sublimation (evaporation) heat per molecule, T_{cl} is the $(CO_2)_N$ cluster temperature, and k_B is the Boltzmann constant. The authors of Refs [195, 197] used the available literature data to estimate parameters entering into formula (4.14) ($\tau_0 \approx 10^{-13}$ s [35], sublimation heat $\Delta E_{ev} = 5.46$ kcal mol^{-1} [186], and $T_{cl} = 100-120$ K [35, 106]) and showed that the lifetime τ varies from several dozen to several hundred microseconds).

Because the detection of molecular and cluster beams by a PED is based on measuring the beam energy and the PED is operated at room temperature, a positive signal is induced on the PED during detection of molecular beams in which the molecular energy (E_b) meets the condition $E_b > k_B T_s$ ($k_B T_s$ is the particle energy on the surface of the PED active element). At the same time, the negative signal is induced on the PED when low-energy molecular beams ($E_b < k_B T_s$) or cluster beams are detected [193]. Generation of the negative signal in the case of detecting cluster beams is due to the fact that clusters dissociate in collisions with the PED surface and the energy needed for their dissociation is removed from the surface. The peculiarities of detection of molecular and cluster beams by a PED are described at greater length in paper [193]. In a word, molecules and clusters induce signals on a PED, which exhibit positive and negative polarity, respectively. Selective vibrational excitation of SF_6 molecules scattered from clusters by an intense pulse of the CO_2 laser results in a significant increase in the molecular internal energy and, therefore, in a stronger signal induced on the detector.

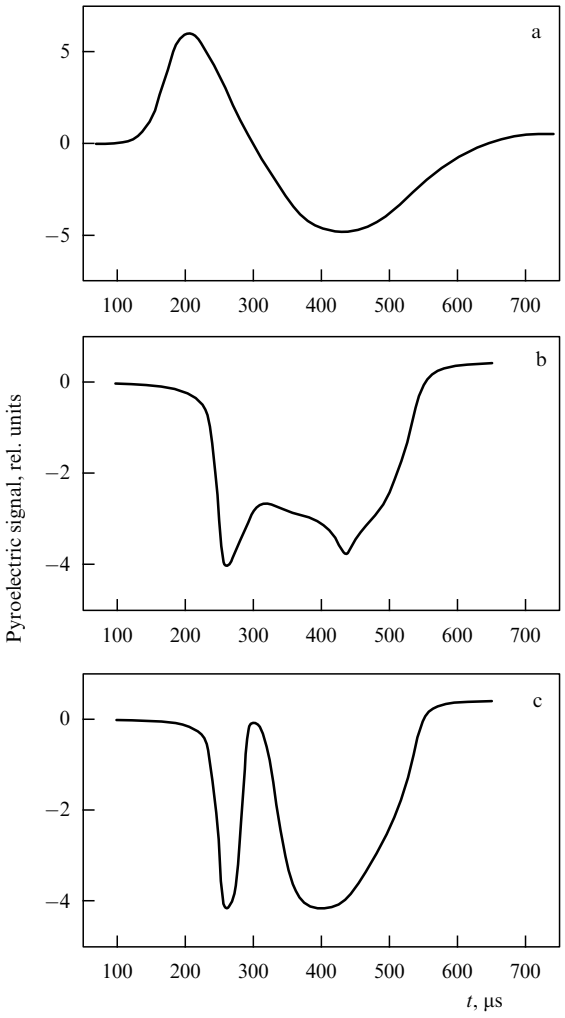

Figure 13. Time evolution of the signals induced by a beam of $(CO_2)_N$ clusters on a PED in the absence of a molecular beam (a), by a cluster beam and SF_6 molecules sublimated from the cluster surface without excitation (b), and by a cluster beam and SF_6 molecules sublimated from the cluster surface upon their vibrational excitation by an intense pulse from a CO_2 laser (c). The CO_2 and SF_6 gas pressures above the nozzle are 4.5 and 2.25 atm, respectively. The distance from the nozzle to the cluster beam detector is 200 mm [184].

4.3.2 Estimation of $(CO_2)_N$ cluster temperature from the IR-MPA spectra of SF_6 molecules sublimated from the cluster surface. As mentioned above, the proposed probe method allows measuring the cluster temperature from the internal (vibrational or rotational) energy of the molecules sublimating from the cluster surface. The internal energy (quantum state) of the molecules can be determined from rotational or vibrational–rotational linear absorption spectra (see Section 3.1). In specific cases (e.g., for SF_6 molecules), the molecular vibrational energy can be estimated from IR-MPA spectra. This possibility was realized in Refs [185, 195] in establishing the temperature of $(CO_2)_N$ nanoparticles in a cluster beam. The results obtained are discussed below.

Figure 13a–c illustrates the time evolution of the signals induced by a beam of $(CO_2)_N$ clusters on a detector placed at an angle of $\theta \approx 2^\circ$ in the absence of a molecular beam (a), by cluster beam and SF_6 molecules sublimated from the cluster surface without the prior excitation (b), and by cluster beam and sublimated SF_6 molecules upon their excitation by a pulse of CO_2 laser (c). First, it is seen from Fig. 13a that the molecules and the clusters induce signals of different polarity on a PED, as ascertained in Ref. [193]. The 'molecular constituent' of the CO_2 beam (positive signal) totally disappears in the presence of the SF_6 beam (Fig. 13b, c) because the molecules and small $(CO_2)_N$ clusters are deflected through wide angles. Figure 13b shows a negative signal from $(CO_2)_N$ clusters in association with a positive signal induced on a PED by SF_6 molecules sublimated from the cluster surfaces. The signal from SF_6 molecules markedly increases upon their resonance excitation by an intense CO_2-laser pulse (Fig. 13c). An additional signal induced on a PED by molecular excitation is a measure of energy absorbed by the molecules from the laser pulse field [168, 169, 189, 191]. Therefore, measurement of the signal as a function of excitation frequency and energy density gives spectral and energy IR-MPA characteristics of SF_6 molecules sublimated from the surface of $(CO_2)_N$ clusters. These characteristics and their comparison with SF_6 characteristics in the initial molecular beam can, in turn, be used to estimate the temperature of $(CO_2)_N$ clusters [195, 197, 198].

Figure 14 displays IR-MPA spectra of SF_6 molecules sublimated from the surface of $(CO_2)_N$ clusters (spectrum *1*) and SF_6 molecules in the original gas-dynamically cooled molecular beam (spectrum *2*). The two spectra are essentially different in that the spectrum *1* has a much narrower low-frequency wing. As reported in Refs [189, 190], this low-frequency wing in the SF_6 MPA spectrum is suppressed as a result of decreasing the molecular vibrational temperature. These observations indicate that the vibrational temperature of the SF_6 molecules sublimated from the surface of $(CO_2)_N$ clusters is much lower than that of SF_6 molecules in the original molecular beam. It was shown in earlier studies [189–191] that the vibrational temperature T_{vib} of SF_6 molecules in a pulsed gas-dynamically cooled molecular beam is less than 150 K, and the rotational temperature $T_{rot} \leqslant 40$ K. Comparison of the spectra in Fig. 14 suggests that SF_6 molecules sublimated from the surface of clusters $(CO_2)_N$ has vibrational temperature $T_{vib} < 150$ K, meaning that the temperature of $(CO_2)_N$ nanoparticles in a cluster beam is $T_{cl} < 150$ K.

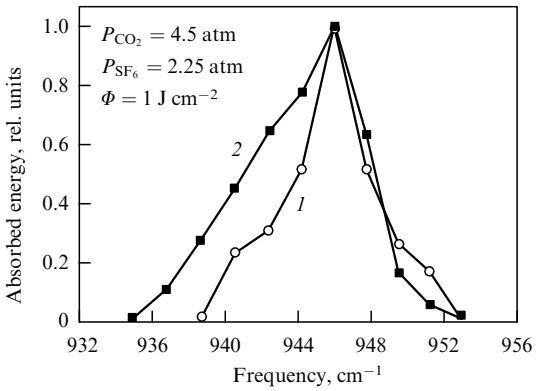

Figure 14. IR-MPA spectra of SF_6 molecules sublimated from the surface of $(CO_2)_N$ clusters (*1*) and in the original gas-dynamically cooled molecular beam (*2*). Exciting radiation energy density is 1 J cm^{-2}. SF_6 gas pressure above the nozzle is 2.25 atm in both cases. The distance from the nozzle to cluster beam detector is 212 mm; the distance between the detector and the beam intersection region is 119 mm (for spectrum *1*), and the distance from the nozzle to detector is 90 mm (for spectrum *2*). For comparison, the two spectra are reduced to the same peak value [185].

4.3.3 Determination of $(CO_2)_N$ cluster temperature from the time-of-flight spectra of SF_6 molecules sublimated from the cluster surface. In order to determine cluster temperature, it is necessary to measure the kinetic or internal energy of the molecules sublimated from the cluster surface. We measured the kinetic energy (velocity) of these molecules. To this effect, the time-of-flight method was applied as described in Refs [191, 199]. The signal induced by sublimated molecules on the detector was amplified by exciting them with an intense pulsed CO_2 laser. The laser beam crossed a flux of sublimated molecules at a distance of 23 mm from the intersection point of the cluster and molecular beams. The time evolution of the signals induced on a PED by vibrationally excited SF_6 molecules sublimated from the surface of clusters $(CO_2)_N$ was measured, and they were compared with the model time-of-flight (TOF) spectra. In order to realize the 'source' $\delta(x_0, t_0)$ of vibrationally excited molecules (x_0 — coordinate of the molecular excitation point, t_0 — instant of excitation), the laser radiation was focused [184, 185] by a cylindrical lens onto a spot whose size in the direction to the detector (along the x-axis) was small (ca 2 mm) compared with the total flight distance $(x_d - x_0)$ from the excitation area to the detector ($\geqslant 40$ mm) (x_d — coordinate of the detector surface). Notice that vibrational excitation did not influence the kinetic energy of the molecules due to the absence of collisions between them in the molecular beam during the time of flight from the excitation area to detector.

Velocity U of the directional motion of SF_6 molecules sublimated from the cluster surfaces and the longitudinal component ($V_{||}$) of their thermal velocity were found from a comparison of experimental findings and the corresponding calculated dependences for model TOF spectra $S(t, y = 0)$ [199]. The model TOF spectrum at point x_d coinciding with the detector surface for particles having the above-set velocity parameters $(U, V_{||})$ is given by the expression [199]

$$S(t, V_{||}) = \int_{t_0}^{t} Y(t - \tau)\, F(\tau)\, \mathrm{d}\tau\,, \tag{4.15}$$

where $F(\tau)$ is the function of the molecular source, modulated by a rectangular pulse, and

$$Y(t, U, V_{||}) = \frac{1}{\sqrt{\pi}\, U^2 V_{||}} \frac{(x_d - x_0)^3}{(t - t_0)^4} \times \exp\left(-\frac{1}{V_{||}^2}\left(\frac{x_d - x_0}{t - t_0} - U\right)^2\right) \tag{4.16}$$

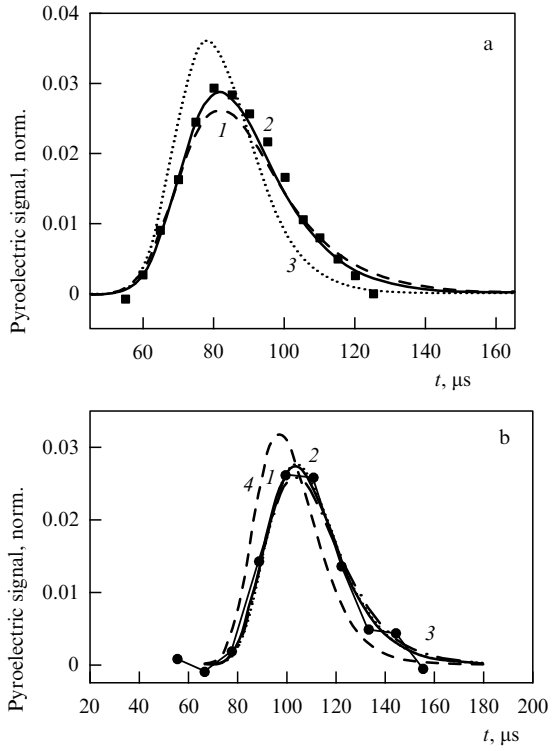

Figure 15. Time-of-flight spectra of vibrationally excited SF_6 molecules sublimated from the $(CO_2)_N$ cluster surface in a cluster beam. Experimental data (squares, circles) are shown together with the results of model calculations using relation (4.16). CO_2 and SF_6 gas pressures above the nozzle are 4.5 and 2.25 atm, respectively. See the text for more details. (a) Angle $\theta = 2°$, distance $(x_d - x_0) = 40$ mm; (b) $\theta = 3.5°$, $x_d - x_0 = 84$ mm. The spectra are normalized to the area [198].

is the response of the detector to a $\delta(x_0, t_0)$ type source [199] (the solution is written out in the normalized form).

The thermal velocity component $V_{||}$ of SF_6 molecules can be used to determine the translational temperature (kinetic energy) of molecules and, therefore, the temperature of $(CO_2)_N$ clusters:

$$V_{||} = \sqrt{\frac{2k_B T_{SF_6}}{m}}, \qquad (4.17)$$

where m is the mass of a SF_6 molecule.

Figure 15a presents the measured time-of-flight spectrum of vibrationally excited SF_6 molecules sublimated from the $(CO_2)_N$ surface (squares) and a few model TOF spectra corresponding to relation (4.16) with different velocity parameters U and $V_{||}$. It should be noted that the experimental TOF signals shown in Fig. 15a represent the difference between the signals from SF_6 molecules vibrationally excited by a laser pulse at point x_0 (analogous to those in Fig. 13c) and the signals from unexcited SF_6 molecules (see Fig 13b). The distance from the excitation area to detector is $x_d - x_0 = 40$ mm. Three spectra with the parameters listed in Table 1 were used to compare experimental data and model spectra. The experimental data are best fitted to the model spectrum *2*. Hence, $U = 430 \pm 20$ m s^{-1}, $V_{||} = 110 \pm 10$ m s^{-1}, and $T_{SF_6} = 105 \pm 15$ K. Based on the assumption that the temperature of SF_6 molecules sublimated from the cluster surface is equal to the temperature of $(CO_2)_N$ clusters, we arrive at $T_{cl} = 105 \pm 15$ K. This value is consistent with the temperature of large $(CO_2)_N$ clusters ($N \geqslant 10^3$) generated in

Table 1

Spectrum	U, m s^{-1}	$V_{||}$, m s^{-1}	T_{SF_6}, K
1	417	120	125
2	428	110	107
3	465	95	80

nozzle sources without a gas-carrier ($T_{cl} \approx 100-120$ K), which was measured by the electron diffraction method [106].

4.3.4 Factors affecting cluster temperature in a beam and results of measurements. Let us consider briefly at the qualitative level the main factors affecting cluster temperature and results of the measurement of this parameter under concrete experimental conditions [198]. To begin with, note that the temperature of clusters with $N \leqslant 200$ monomers rather strongly depends on their size [35, 39]. It decreases as the size curtails. In contrast, the temperature increases with the growth of clusters because they accumulate condensation heat. On the other hand, large (hot) clusters formed in a cluster beam cool after condensation stops due to the evaporation (sublimation) of monomers from the cluster surface [39] (see also Section 3.2).

Furthermore, the authors of Refs [184, 185, 198] experimented with integrated cluster-size distribution instead of clusters of a certain size. Clusters produced in nozzle sources are characterized by logarithmically normal distribution [1, 187, 188], with the distribution width being roughly equal to the mean cluster size. For this reason, the measurements were made with a rather wide spread of cluster sizes (presumably in the range $N \approx 10 - 10^3$). The capture of single SF_6 molecules by clusters of different sizes caused the clusters to deflect through different angles. Consequently, the measured cluster temperature depends on the angle θ through which the clusters deflect (see Fig. 12), i.e., the greater the angle θ, the lower the measured temperature. Moreover, cluster temperature decreases with increasing distance from the molecule capture area to the detector as a result of cluster cooling by evaporation (sublimation) [39]. All these factors influence the results of measurements. By way of example, it was shown in Ref. [198] that the measured temperature of sublimated SF_6 molecules [hence $(CO_2)_N$ clusters] was $T_{cl} = 85 \pm 10$ K, when the angle θ increased from about 2° to 3.5° and the molecular excitation area–detector distance $(x_d - x_0)$ increased from 40 to 84 mm (Fig. 15b). The model TOF spectra shown in Fig. 15b have the parameters given in Table 2.

It should be noted that fragmentation (evaporation) is the most efficient cooling channel for hot or excited clusters compared with other energy relaxation channels (emission of equilibrium radiation, electrons, and ions) [35, 39]. It was shown that a $(CO_2)_N$ cluster composed of $N = 100$ particles cools by $\Delta T \approx 6.8$ K as it loses one molecule through sublimation from its surface (CO_2 heat capacity is 8.87 cal mol^{-1} K^{-1} [186], sublimation energy is 6.03 kcal mol^{-1} [186]); evaporation of an SF_6 molecule results

Table 2

Spectrum	U, m s^{-1}	$V_{||}$, m s^{-1}	T_{SF_6}, K
1	436	95	79.3
2	435	93	76
3	430	100	87.9
4	470	92	75

in cluster cooling by $\Delta T \approx 6.2$ K. At the same time, the capture of an SF_6 molecule from the molecular beam (the energy of one molecule in a pulsed beam is ca 0.17 eV [168, 200, 201]) results in a rise in temperature of a $(CO_2)_N$ cluster containing $N = 100$ or $N = 10$ particles by $\Delta T \approx 4.5$ K and $\Delta T \approx 45$ K, respectively. Therefore, the capture of SF_6 molecules sharply rises the probability of fragmentation of small clusters.

The influence of $(CO_2)_N$ cluster velocity distribution in a beam on the results of measurement of the velocity of SF_6 molecules sublimated from the cluster surface (hence, cluster temperature) was estimated in Ref. [198] based on the relationship between the experimentally found longitudinal component of molecular thermal velocity ($V_{||}$), its real value ($V_{||,\,\mathrm{real}}$), and the longitudinal component of cluster thermal velocity ($V_{||,\,\mathrm{cl}}$). The root-mean-square values of these quantities are related by the expression

$$\langle V_{||}^2 \rangle = \langle V_{||,\,\mathrm{real}}^2 \rangle + \langle V_{||,\,\mathrm{cl}}^2 \rangle \,. \tag{4.18}$$

The longitudinal component of thermal velocity of $(CO_2)_N$ clusters in a beam measured by the time-of-flight method was $V_{||,\,\mathrm{cl}} \approx 16$ m s^{-1}, or significantly smaller than that of sublimated SF_6 molecules ($V_{||} \approx 110$ m s^{-1} and $V_{||} \approx 95$ m s^{-1} in the cases illustrated in Figs 15a and 15b, respectively). In other words, the factor under consideration had practically no effect on the results of cluster temperature measurements.

5. Conclusion

The results of experimental and theoretical studies in the above-cited literature sources indicate that the temperature (internal energy) of clusters and nanoparticles is an important physical characteristic determining many of their properties and the character of processes with their participation. Therefore, the development of methods for the measurement of cluster and nanoparticle temperatures remains a topical issue.

Earlier techniques for this purpose (electron diffraction, optical, and thermodynamic methods) permit determining the temperature of large clusters ($N \geqslant 10^3$) with a rather good accuracy. Recently proposed kinetic methods for measuring the temperature of free clusters and nanoparticles in molecular beams make it possible, in principle, to determine the temperature of clusters and nanoparticles of practically any size and composition.

The method for determining sodium cluster temperature in a beam [124] described in Section 4.1 is based on the measurement of recoil (escape from the beam) energy of daughter fragments resulting from cluster dissociation. Its advantage is the possibility of measuring the temperature of clusters of a given size. At the same time, its application appears to be restricted to specific conditions, in particular, to the measurement of magic cluster temperature when the influence of neighbor-sized clusters in the beam can be neglected.

The method for determining the temperature of van der Waals $(CF_3I)_N$ clusters [167] described in Section 4.2 and based on the measurement of kinetic energy (velocity) of dissociation fragments (CF_3I molecules) can find, in principle, a wider application. However, it is limited by the lack of suitable lasers and studied schemes of photoionization detection of cluster dissociation fragments. The method allows not only determining the temperature of IR laser-excited clusters at different excitation energy densities but also studying cluster decay kinetics. For example, it was shown in Ref. [167] that resonant excitation of CF_3I molecules by IR radiation of a pulsed CO_2 laser triggers breakdown of $(CF_3I)_N$ clusters via successive evaporation of molecules. There is no significant 'overheating' of clusters. Excited clusters dissociate rather fast (in less than 10^{-8} s). Due to this, evaporation of $(CF_3I)_N$ clusters under the realized conditions of the experiment (excitation rate, IR pulse duration) occurs in a stationary or close to stationary mode.

An advantage of the probe method [184, 185, 198] described in Section 4.3 is that it is nondestructive and can be used to measure the temperature of unexcited clusters and nanoparticles in a beam. However, for this method to be realized, the heat of evaporation of the probe thermometer-particle from the cluster surface must be lower than that of the cluster particles themselves. The method is universally applicable if this condition is met. For example, it permits determining the temperature of practically any clusters or nanoparticles in a beam using atoms or molecules with very low evaporation (sublimation) energy as probe thermometers, viz. He, Ne, H_2, N_2, CO, and CH_4. Also, the large scattering angle of light atoms (molecules) sublimating from the cluster surfaces makes it easier to measure the transverse, rather than longitudinal, component of their thermal velocity.

To conclude, the rather low vibrational temperature of SF_6 molecules sublimated from the cluster surface compared with that in the original beam (see Refs [184, 185, 198]) suggests that the captured SF_6 molecules reach perfect thermal equilibrium with $(CO_2)_N$ clusters while they remain on their surfaces. For this reason, they may be regarded as miniature molecular thermometers carrying real information on cluster temperature.

The author is grateful to V N Lokhman and A N Petin for assistance in preparing the drawings. The valuable comments by the reviewer are appreciated. This work was supported in part by RFBR (grants 07-02-00165 and 09-02-00531).

References

1. Pauly H *Atom, Molecule, and Cluster Beams* Vol. 2 *Cluster Beams, Fast and Slow Beams, Accessory Equipment, and Applications* (New York: Springer, 2000)
2. Scoles G (Ed.) *Atomic and Molecular Beam Methods* Vol. 1 (New York: Oxford Univ. Press, 1988)
3. Scoles G (Ed.) *Atomic and Molecular Beam Methods* Vol. 2 (New York: Oxford Univ. Press, 1992)
4. Bernstein E R (Ed.) *Atomic and Molecular Clusters* (Amsterdam: Elsevier, 1990)
5. Jena P, Khanna S N, Rao B K (Eds) *Physics and Chemistry of Finite Systems*: *From Clusters to Crystals* (Dordrecht: Kluwer Acad. Publ., 1992)
6. de Heer W A *Rev. Mod. Phys.* **65** 611 (1993)
7. Haberland H (Ed.) *Clusters of Atoms and Molecules*: *Theory, Experiment, and Clusters of Atoms* (Heidelberg: Springer-Verlag, 1994)
8. Klabunde K J *Free Atoms, Clusters, and Nanoscale Particles* (San Diego: Academic Press, 1994)
9. Smirnov B M *Usp. Fiz. Nauk* **164** 1165 (1994) [*Phys. Usp.* **37** 1079 (1994)]
10. Martin T P (Ed.) *Large Clusters of Atoms and Molecules* (Dordrecht: Kluwer Acad. Publ., 1996)
11. Alivisatos A P *J. Phys. Chem.* **100** 13226 (1996)
12. Castleman A W (Jr.), Bowen K H (Jr.) *J. Phys. Chem.* **100** 12911 (1996)

13. Christen W, Even U *J. Phys. Chem. A* **102** 9420 (1998)
14. Herschbach D *Rev. Mod. Phys.* **71** S411 (1999)
15. Smalley R E *Rev. Mod. Phys.* **69** 723 (1997); *Usp. Fiz. Nauk* **168** 323 (1998)
16. Curl R F *Rev. Mod. Phys.* **69** 691 (1997); *Usp. Fiz. Nauk* **168** 331 (1998)
17. Kroto H *Rev. Mod. Phys.* **69** 703 (1997); *Usp. Fiz. Nauk* **168** 343 (1998)
18. Perez A et al. *J. Phys. D* **30** 709 (1997)
19. Smirnov B M *Usp. Fiz. Nauk* **171** 1291 (2001) [*Phys. Usp.* **44** 1229 (2001)]
20. Smirnov B M *Usp. Fiz. Nauk* **173** 609 (3003) [*Phys. Usp.* **46** 589 (2003)]
21. Ditmire T et al. *Phys. Rev. A* **53** 3379 (1996)
22. Zweiback J et al. *Phys. Plasmas* **9** 3108 (2002)
23. Northby J A *J. Chem. Phys.* **115** 10065 (2001)
24. Callegari C et al. *J. Chem. Phys.* **115** 10090 (2001)
25. Stienkemeier F, Vilesov A F *J. Chem. Phys.* **115** 10119 (2001)
26. Toennies J P, Vilesov A F, Whaley K B *Phys. Today* **54** (2) 31 (2001)
27. Toennies J P, Vilesov A F *Angew. Chem. Int. Ed.* **43** 2622 (2004)
28. Makarov G N *Usp. Fiz. Nauk* **174** 225 (2004) [*Phys. Usp.* **47** 217 (2004)]
29. Yamada I, Toyoda N *Nucl. Instrum. Meth. Phys. Res. B* **232** 195 (2005)
30. Berry R S, Smirnov B M *Usp. Fiz. Nauk* **175** 367 (2005) [*Phys. Usp.* **48** 345 (2005)]
31. Makarov G N *Usp. Fiz. Nauk* **176** 121 (2006) [*Phys. Usp.* **49** 117 (2006)]
32. Popok V N, Campbell E E B *Rev. Adv. Mater. Sci.* **11** 19 (2006)
33. Eletskii A V *Usp. Fiz. Nauk* **177** 233 (2007) [*Phys. Usp.* **50** 225 (2007)]
34. Krainov V P, Smirnov B M, Smirnov M B *Usp. Fiz. Nauk* **177** 953 (2007) [*Phys. Usp.* **50** 907 (2007)]
35. Makarov G N *Usp. Fiz. Nauk* **178** 337 (2008) [*Phys. Usp.* **51** 319 (2008)]
36. Kresin V Z, Ovchinnikov Yu N *Usp. Fiz. Nauk* **178** 449 (2008) [*Phys. Usp.* **51** 427 (2008)]
37. Makarov G N *Usp. Fiz. Nauk* **179** 487 (2009) [*Phys. Usp.* **52** 461 (2009)]
38. Berry R S, Smirnov B M *Usp. Fiz. Nauk* **179** 147 (2009) [*Phys. Usp.* **52** 137 (2009)]
39. Makarov G N *Usp. Fiz. Nauk* **180** 185 (2010) [*Phys. Usp.* **53** 179 (2010)]
40. Siegel R W, Hu E, Roco M C (Eds) *Nanostructure Science and Technology* (Dordrecht: Kluwer Acad. Publ., 1999)
41. Renn O, Roco M C *J. Nanopart. Res.* **8** 153 (2006)
42. Rubahn H G *Nanophysik und Nanotechnologie* (Stuttgart: Teubner Verlag, 2002)
43. Edelstein A S, Cammarata R C (Eds) *Nanomaterials: Synthesis, Properties, and Applications* (Bristol: Institute of Physics Publ., 1996)
44. Moro R et al. *Science* **300** 1265 (2003)
45. Moro R et al. *Phys. Rev. Lett.* **93** 086803 (2004)
46. Andersen K E et al. *Phys Rev. B* **73** 125418 (2006)
47. Xu X et al. *Phys Rev. B* **75** 085429 (2007)
48. Berry R S, Smirnov B M *Zh. Eksp. Teor. Fiz.* **117** 562 (2000) [*JETP* **90** 491 (2000)]
49. Berry R S, Smirnov B M *Zh. Eksp. Teor. Fiz.* **125** 414 (2004) [*JETP* **98** 366 (2004)]
50. Bixon M, Jortner J *J. Chem. Phys.* **91** 1631 (1989)
51. Labastie P, Whetten R L *Phys. Rev. Lett.* **65** 1567 (1990)
52. Wales D J *Mol. Phys.* **78** 151 (1993)
53. Wales D J, Berry R S *Phys. Rev. Lett.* **73** 2875 (1994)
54. Umirzakov I H *Phys. Rev. E* **60** 7550 (1999)
55. Mülken O, Stamerjohanns H, Borrmann P *Phys. Rev. E* **64** 047105 (2001)
56. Schmidt M et al. *Phys. Rev. Lett.* **79** 99 (1997)
57. Schmidt M et al. *Nature* **393** 238 (1998)
58. Schmidt M et al. *Phys. Rev. Lett.* **86** 1191 (2001)
59. Schmidt M et al. *Phys. Rev. Lett.* **87** 203402 (2001)
60. Gobet F et al. *Phys. Rev. Lett.* **89** 183403 (2002)
61. Reyes-Nava J A, Garzón I L, Michaelian K *Phys. Rev. B* **67** 165401 (2003)
62. Jellinek J, Beck T L, Berry R S *J. Chem. Phys.* **84** 2783 (1986)
63. Beck T L, Jellinek J, Berry R S *J. Chem. Phys.* **87** 545 (1987)
64. Davis H L, Jellinek J, Berry R S *J. Chem. Phys.* **86** 6456 (1987)
65. Berry R S, Jellinek J, Natanson G *Phys. Rev. A* **30** 919 (1984)
66. Beck T L, Berry R S *J. Chem. Phys.* **88** 3910 (1988)
67. Wales D J, Berry R S *J. Chem. Phys.* **92** 4283 (1990)
68. Berry R S *Chem. Rev.* **93** 2379 (1993)
69. Berry R S *Nature* **393** 212 (1998)
70. Berry R S, in *Theory of Atomic and Molecular Clusters* (Ed. J Jellinek) (Berlin: Springer-Verlag, 1999) p. 1
71. Cheng H-P, Berry R S *Phys. Rev. A* **45** 7969 (1992)
72. Kunz R E, Berry R S *Phys. Rev. Lett.* **71** 3987 (1993)
73. Kunz R E, Berry R S *Phys. Rev. E* **49** 1895 (1994)
74. Wales D J *Chem. Phys. Lett.* **166** 419 (1990)
75. Berry R S, Smirnov B M *Zh. Eksp. Teor. Fiz.* **127** 1282 (2005) [*JETP* **100** 1129 (2005)]
76. Berry R S et al. *Adv. Chem. Phys.* **90** 75 (1988)
77. Briant C L, Burton J J *J. Chem. Phys.* **63** 2045 (1975)
78. Damgaard Kristensen W, Jensen E J, Cotterill M R J *J. Chem. Phys.* **60** 4161 (1974)
79. Etters R D, Kaelberrer J B *Phys. Rev. A* **11** 1068 (1975)
80. Kaelberrer J B, Etters R D *J. Chem. Phys.* **66** 3233 (1977)
81. Etters R D, Kaelberrer J B *J. Chem. Phys.* **66** 5112 (1977)
82. Berry R S, Smirnov B M *Zh. Eksp. Teor. Fiz.* **122** 298 (2002) [*JETP* **95** 255 (2002)]
83. Berry R S, Smirnov B M *J. Chem. Phys.* **114** 6816 (2001)
84. Vekhter B et al. *J. Chem. Phys.* **106** 4644 (1997)
85. Wales D J, Ohmine I *J. Chem. Phys.* **98** 7245 (1993)
86. Wales D J *Adv. Chem. Phys.* **115** 1 (2000)
87. Wales D J *Energy Landscapes* (Cambridge: Cambridge Univ. Press, 2003)
88. Harms J et al. *J. Mol. Spectrosc.* **185** 204 (1996)
89. Brink D M, Stringari S *Z. Phys. D* **15** 257 (1990)
90. Bulgac A *Czech. J. Phys.* **48** 697 (1998)
91. Li Y B, Blaisten-Barojas E, Papaconstantopoulos D A *Phys. Rev. B* **57** 15519 (1998)
92. Bréchignac C et al. *Phys. Rev. Lett.* **89** 183402 (2002)
93. Bréchignac C et al. *Phys. Rev. A* **68** 063202 (2003)
94. Wan Z et al. *J. Chem. Phys.* **99** 5858 (1993)
95. Wurz P, Lykke K R *J. Phys. Chem.* **96** 10129 (1992)
96. Ho J et al. *J. Chem. Phys.* **99** 140 (1993)
97. Boyukata M et al. *Int. J. Mod. Phys.* **16** 295 (2005)
98. Geé C et al. *J. Phys. Chem.* **100** 13421 (1996)
99. Geé C et al. *J. Chem. Phys.* **107** 4194 (1997)
100. Lugovoj E, Toennies J P, Vilesov A *J. Chem. Phys.* **112** 8217 (2000)
101. Lallement A et al. *Chem. Phys. Lett.* **189** 182 (1992)
102. Chaparro S A et al. *J. Appl. Phys.* **87** 2245 (2000)
103. Yamaguchi N et al. *Thin Solid Films* **345** 34 (1999)
104. Yamaguchi N, Terashima K, Yoshida T *J. Mater. Sci. Lett.* **17** 2067 (1998)
105. Farges J et al. *Surf. Sci.* **106** 95 (1981)
106. Torchet G, Docteur es-Sciences Thesis (Paris: Paris Univ., 1978)
107. Torchet G et al. *J. Chem. Phys.* **105** 3671 (1996)
108. Kovalenko S I et al. *J. Cryst. Growth* **191** 553 (1998)
109. Calvo F, Torchet G, de Feraudy M-F *J. Chem. Phys.* **111** 4650 (1999)
110. Rohlfing E A *J. Chem. Phys.* **89** 6103 (1988)
111. Mitzner R, Campbell E E B *J. Chem. Phys.* **103** 2445 (1995)
112. Frenzel U et al. *Z. Phys. D* **40** 108 (1997)
113. Vostrikov A A, Dubov D Yu, Agarkov A A *Pis'ma Zh. Eksp. Teor. Fiz.* **63** 915 (1996) [*JETP Lett.* **63** 963 (1996)]
114. Makarov G N, Petin A N *Chem. Phys. Lett.* **426** 464 (2006)
115. Makarov G N, Petin A N *Zh. Eksp. Teor. Fiz.* **130** 804 (2006) [*JETP* **103** 697 (2006)]
116. Gspann J *Z. Phys D* **3** 143 (1986)
117. Gspann J, in *Physics of Electronic and Atomic Collisions* (Ed. S Datz) (Amsterdam: North-Holland, 1982) p. 79
118. Klots C E *J. Chem. Phys.* **83** 5854 (1985)
119. Klots C E *Z. Phys. D* **5** 83 (1987)
120. Klots C E *J. Chem. Phys.* **90** 4470 (1989)
121. Klots C E *Z. Phys. D* **21** 335 (1991)
122. Klots C E *Nature* **327** 222 (1987)
123. Klots C E *J. Phys. Chem.* **92** 5864 (1988)
124. Brockhaus P et al. *Phys. Rev. A* **59** 495 (1999)

125. Jundt G et al. *Chem. Phys. Lett.* **370** 504 (2003)
126. Makarov G N *Usp. Fiz. Nauk* **176** 1155 (2006) [*Phys. Usp.* **49** 1131 (2006)]
127. Heszler P, Carlsson J O, Demirev P *J. Chem. Phys.* **107** 10440 (1997)
128. Frenzel U et al. *Surf. Rev. Lett.* **3** 505 (1996)
129. Heszler P, Carlsson J O, Demirev P *Phys. Rev. B* **53** 12541 (1996)
130. Mitzner R, Campbell E E B *Surf. Rev. Lett.* **3** 759 (1996)
131. Agarkov A A et al. *Eur. Phys. J. D* **9** 331 (1999)
132. Vostrikov A A, Agarkov A A, Dubov D Yu *Zh. Tekh. Fiz.* **70** (7) 102 (2000) [*Tech. Phys.* **45** 915 (2000)]
133. Vostrikov A A, Dubov D Yu, Agarkov A A *Teplofiz. Vys. Temp.* **39** 26 (2001) [*High Temp.* **39** 22 (2001)]
134. Foltin M et al. *J. Chem. Phys.* **98** 9624 (1993)
135. Christian J F, Wan Z, Anderson S L *J. Phys. Chem.* **96** 10597 (1992)
136. Wan Z, Christian J F, Anderson S L *J. Chem. Phys.* **96** 3344 (1992)
137. Frenzel U, Roggenkamp A, Kreisle D *Chem. Phys. Lett.* **240** 109 (1995)
138. Gafner Yu Ya et al. *Fiz. Tverd. Tela* **47** 1304 (2005) [*Phys. Solid State* **47** 1353 (2005)]
139. Ascencio J A et al. *Surf. Sci.* **396** 349 (1998)
140. Borman V D et al. *Zh. Eksp. Teor. Fiz.* **130** 984 (2006) [*JETP* **103** 850 (2006)]
141. Dolbec R et al. *Phys. Rev. B* **70** 201406(R) (2004)
142. Sibener S J, Hislop P, LBL Report, Part VII, Advanced Isotope Separation Technology (1978) p. 470
143. Klekamp A, Umbach E *Surf. Sci.* **249** 75 (1991)
144. Makarov G N, Petin A N *Pis'ma Zh. Eksp. Teor. Fiz.* **83** 115 (2006) [*JETP Lett.* **83** 87 (2006)]
145. Makarov G N, Petin A N *Kvantovaya Elektron.* **36** 889 (2006) [*Quantum Electron.* **36** 889 (2006)]
146. Makarov G N, Petin A N *Opt. Spektrosk.* **102** 434 (2007) [*Opt. Spectrosc.* **102** 388 (2007)]
147. Haberland H et al. *Phys. Rev. Lett.* **94** 035701 (2005)
148. Schmidt M et al. *Phys. Rev. Lett.* **90** 103401 (2003)
149. Robinson P J, Holbrook K A *Unimolecular Reactions* (London: Wiley, 1972) [Translated into Russian (Moscow: Mir, 1975)]
150. Eyring H, Lin S H, Lin S M *Basic Chemical Kinetics* (New York: Wiley, 1980)
151. Näher U, Hansen K *J. Chem. Phys.* **101** 5367 (1994)
152. Hansen K, Campbell E E B *Int. J. Mass Spectrom.* **233** 215 (2004)
153. Hansen K *Chem. Phys. Lett.* **383** 270 (2004)
154. Andersen J U, Bonderup E, Hansen K *J. Chem. Phys.* **114** 6518 (2001)
155. Stenfalk J, Hansen K *Eur. Phys. J. D* **43** 101 (2007)
156. Borggreen J et al. *Phys. Rev. A* **62** 013202 (2000)
157. Chandezon F et al. *Chem. Phys. Lett.* **277** 450 (1997)
158. Martin T P et al. *Chem. Phys. Lett.* **183** 119 (1991)
159. Martin T P et al. *Chem. Phys. Lett.* **186** 53 (1991)
160. Pedersen J et al. *Nature* **353** 733 (1991)
161. Bréchignac C et al. *Phys. Rev. Lett.* **68** 3916 (1992)
162. Farges J *J. Cryst. Growth* **31** 79 (1975)
163. Kresin V V et al. *Phys. Rev. A* **57** 383 (1998)
164. Blatt J M, Weisskopf V F *Theoretical Nuclear Physics* (Heidelberg: Springer-Verlag, 1979)
165. Ericson T *Adv. Phys.* **9** 425 (1960)
166. Bréchignac C et al. *J. Chem. Phys.* **90** 1492 (1989)
167. Lokhman V N, Ogurok D D, Ryabov E A *Zh. Eksp. Teor. Fiz.* **135** 835 (2009) [*JETP* **108** 727 (2009)]
168. Makarov G N *Usp. Fiz. Nauk* **173** 913 (2003) [*Phys. Usp.* **46** 889 (2003)]
169. Makarov G N *Usp. Fiz. Nauk* **175** 41 (2005) [*Phys. Usp.* **48** 37 (2005)]
170. Fuss W *Spectrochim. Acta A* **38** 829 (1982)
171. Bagratashvili V N et al. *Zh. Eksp. Teor. Fiz.* **77** 2238 (1979) [*Sov. Phys. JETP* **50** 1075 (1979)]
172. Apatin V M, Makarov G N *Kvantovaya Elektron.* **10** 1435 (1983) [*Sov. J. Quantum Electron.* **13** 932 (1983)]
173. Makarov G N et al. *Kvantovaya Elektron.* **25** 545 (1998) [*Quantum Electron.* **28** 530 (1998)]
174. Makarov G N *Pis'ma Zh. Tekh. Fiz.* **24** (23) 35 (1998) [*Tech. Phys. Lett.* **24** 921 (1998)]
175. Makarov G N, Malinovsky D E, Ogurok D D *Laser Chem.* **17** 205 (1998)
176. Makarov G N, Malinovskii D E, Ogurok D D *Zh. Tekh. Fiz.* **69** (1) 35 (1999) [*Tech. Phys.* **44** 31 (1999)]
177. Lokhman V N, Ogurok D D, Ryabov E A *Chem. Phys.* **333** 85 (2007)
178. Lokhman V N, Ogurok D D, Ryabov E A *Zh. Eksp. Teor. Fiz.* **130** 5 (2006) [*JETP* **103** 1 (2006)]
179. Downie P, Powis I *Faraday Discuss.* **115** 103 (2000)
180. Lokhman V N, Ogurok D D, Ryabov E A *Eur. Phys. J. D* **46** 59 (2008)
181. Buck U *J. Phys. Chem.* **98** 5190 (1994)
182. Lokhman V N, Ogurok D D, Ryabov E A *Zh. Tekh. Fiz.* **75** (7) 29 (2005) [*Tech. Phys.* **50** 846 (2005)]
183. Vostrikov A A, Dubov D Yu *Zh. Eksp. Teor. Fiz.* **125** 222 (2004) [*JETP* **98** 197 (2004)]
184. Makarov G N, Petin A N *Pis'ma Zh. Eksp. Teor. Fiz.* **90** 712 (2009) [*JETP Lett.* **90** 642 (2010)]
185. Makarov G N, Petin A N *Chem. Phys. Lett.* **484** 14 (2009)
186. Nikol'skii B P (Ed.-in-Chief) *Spravochnik Khimika* (Chemist's Reference Book) 2nd ed. (Leningrad–Moscow: Goskhimizdat, 1962)
187. Lewerenz M, Schilling B, Toennies J P *Chem. Phys. Lett.* **206** 381 (1993)
188. Lewerenz M, Schilling B, Toennies J P *J. Chem. Phys.* **102** 8191 (1995)
189. Apatin V M, Makarov G N *Zh. Eksp. Teor. Fiz.* **84** 15 1983 [*Sov. Phys. JETP* **57** 8 (1983)]
190. Apatin V M, Makarov G N *Kvantovaya Elektron.* **9** 1668 (1982) [*Sov. J. Quantum Electron.* **12** 1067 (1982)]
191. Apatin V M et al. *Appl. Phys. B* **29** 273 (1982)
192. Gentry W R, Giese C F *Rev. Sci. Instrum.* **49** 595 (1978)
193. Makarov G N, Petin A N *Zh. Eksp. Teor. Fiz.* **134** 851 (2008) [*JETP* **107** 725 (2008)]
194. McDowell R S et al. *Spectrochim. Acta A* **42** 351 (1986)
195. Makarov G N, Petin A N *Pis'ma Zh. Eksp. Teor. Fiz.* **89** 468 (2009) [*JETP Lett.* **89** 404 (2009)]
196. Frenkel' Ya I *Kineticheskaya Teoriya Zhidkostei* (The Quantum Theory of Liquids) (Moscow–Leningrad: Izd. AN SSSR, 1945) [Translated into English: *Kinetic Theory of Liquids* (Oxford: The Univ. Press, 1946)]
197. Makarov G N, Petin A N *Kvantovaya Elektron.* **39** 1054 (2009) [*Quantum Electron.* **39** 1054 (2009)]
198. Makarov G N, Petin A N *Zh. Eksp. Teor. Fiz.* **137** 646 (2010) [*JETP* **110** 568 (2010)]
199. Eldridge B N, Yu M L *Rev. Sci. Instrum.* **58** 1014 (1987)
200. Makarov G N *Chem. Phys.* **290** 137 (2003)
201. Makarov G N *Zh. Eksp. Teor. Fiz.* **123** 276 (2003) [*JETP* **96** 241 (2003)]